HHS Public Access

Author manuscript

Nat Cell Biol. Author manuscript; available in PMC 2021 March 21.

Protein Quality Control Through Endoplasmic Reticulum-Associated Degradation Maintains Hematopoietic Stem Cell Identity and Niche Interactions

Longyong Xu[1,2,13], **Xia Liu**[1,2,13], **Fanglue Peng**[1,2,13], **Weijie Zhang**[1,2,13], **Liting Zheng**[3], **Yao Ding**[1,2], **Tianpeng Gu**[1,4], **Kaosheng Lv**[5,6], **Jin Wang**[7], **Laura Ortinau**[8], **Tianyuan Hu**[8], **Xiangguo Shi**[8], **Guojun Shi**[9], **Ge Shang**[1], **Shengyi Sun**[10], **Takao Iwawaki**[11], **Yewei Ji**[9], **Wei Li**[1,2], **Jeffrey M. Rosen**[1,2], **Xiang H.-F. Zhang**[1,2], **Dongsu Park**[8], **Stanley Adoro**[12], **Andre Catic**[1,2], **Wei Tong**[5,6], **Ling Qi**[9], **Daisuke Nakada**[8], **Xi Chen**[1,2]

[1.]Department of Molecular and Cellular Biology, Baylor College of Medicine, Houston, Texas 77030, USA

[2.]Lester and Sue Smith Breast Center and Dan L Duncan Comprehensive Cancer Center, Baylor College of Medicine, Houston, Texas 77030, USA

[3.]Department of Biochemistry & Molecular Biology, Baylor College of Medicine, Houston, Texas 77030, USA

[4.]Stem Cells and Regenerative Medicine Center, Baylor College of Medicine, Houston, TX 77030, USA

[5.]Division of Hematology, Children′s Hospital of Philadelphia, Philadelphia, PA 19104, USA

[6.]Department of Pediatrics, Perelman School of Medicine at the University of Pennsylvania, Philadelphia, PA 19104, USA

[7.]Department of Pharmacology and Chemical Biology, Baylor College of Medicine, Houston, TX 77030, USA

[8.]Department of Molecular and Human Genetics, Baylor College of Medicine, Houston, TX 77030, USA

[9.]Department of Molecular and Integrative Physiology, Department of Internal Medicine, University of Michigan Medical School, Ann Arbor, MI 48105, USA

[10.]Center for Molecular Medicine and Genetics, Wayne State University School of Medicine, Detroit, MI 48201, USA

Corresponding author: Xi Chen, Ph.D., Department of Molecular and Cellular Biology, Lester and Sue Smith Breast Center and Dan L Duncan Comprehensive Cancer Center, Baylor College of Medicine, One Baylor Plaza, MS: BCM130, Debakey Building, BCMM-M626, Houston, TX 77030, USA; Phone 713-798-4398; FAX 713-790-1275; Xi.Chen@bcm.edu.

[11.]Division of Cell Medicine, Department of Life Science, Medical Research Institute, Kanazawa Medical University, Uchinada, Japan

[12.]Department of Pathology, Case Western Reserve University School of Medicine, Cleveland, OH 44106, USA

[13.]These authors contributed equally to this work

Abstract

Stem cells need to be protected from genotoxic and proteotoxic stress to maintain a healthy pool throughout life[1–3]. Little is known about the proteostasis mechanism that safeguards the stem cells. Here, we report Endoplasmic Reticulum-Associated Degradation (ERAD) as a protein quality checkpoint that controls hematopoietic stem cell (HSC)-niche interaction and determines the fate of HSC. SEL1L-HRD1 complex, the most conserved branch of ERAD[4], is highly expressed in HSC. Deletion of *Sel1l* led to niche displacement of HSC, complete loss of HSC identity, and allowed highly efficient donor-HSC engraftment without irradiation. Mechanistic studies identified MPL, the master regulator of HSC identity[5], as a bona-fide ERAD substrate that became aggregated in the ER upon ERAD deficiency. Restoration of MPL signaling with an agonist partially rescued the number and reconstitution capacity of *Sel1l*-deficient HSCs. Our study defines ERAD as an essential proteostasis mechanism to safeguard a healthy stem cell pool through regulating the stem cell-niche interaction.

Our analysis revealed that the expression of ERAD pathway components was markedly enriched in mouse long-term repopulating HSCs[6, 7] (LT-HSCs; Fig. 1a, b and Extended Data Fig. 1 and 2). ERAD is the principal protein quality control machinery responsible for targeting misfolded proteins in the ER for cytosolic proteasomal degradation[4]. The SEL1L-HRD1 complex, which consists of the E3 ubiquitin ligase HRD1 and its adaptor protein SEL1L, is the most conserved branch of ERAD[4].

We generated an inducible knockout mouse model *Sel1l^flox/flox^/Mx1-cre* (*Sel1l^Mx1^*-KO) to delete *Sel1l* from hematopoietic cells via injections of polyinosinic-polycytidylic acid (poly(I:C)). *Sel1l* depletion had little acute effect on the BM cellularity (Extended Data Fig. 3a, b). Serial analysis of HSCs revealed that *Sel1l* depletion led to progressive decline of steady-state HSCs after transient expansion at 1-week (Fig. 1c). The committed progenitors and the mature cells in BM also progressively declined with *Sel1l* deletion (Extended Data Fig. 3c–f). As a consequence, *Sel1l*-KO led to anemia 30 weeks after poly(I:C) injection (Extended Data Fig. 3g–n).

We also generated *Sel1l^flox/flox^/Vav-icre* (*Sel1l^Vav^*-KO) mice. Deletion of *Sel1l* in *Sel1l^Vav^*-KO mice had little effect on the body weight and BM cellularity of 8-week-old mice (Extended Data Fig. 4a–d), but substantially reduced the steady-state HSCs compared to control littermates (Fig. 1d, e and Extended Data Fig. 4e). In contrast, *Sel1l* deletion did not impair the *in vitro* colony-forming activity of progenitors from 8-week-old mice (Extended Data Fig. 4f). In 50-week-old *Sel1l^Vav^*-KO mice, more than 95% of HSCs, as well as the committed progenitors, were lost in the BM compared with control littermates (Fig. 1d, e, and Extended Data Fig. 4g–j). As a consequence, *Sel1l* deletion led to anemia and early

lethality (Extended Data Fig. 4k, l). These data demonstrate that *Sel1l* deletion leads to HSC exhaustion, indicating that SEL1L is indispensable for the maintenance of steady-state HSCs.

Cell cycle analysis showed that *Sel1l* deletion led to decreased HSCs in G0 and increased the proportion of HSCs in G1 (Fig. 1f, g). *Sel1l*^{Vav}-KO HSCs also exhibited a significant increase in 5-bromodeoxyuridine (BrdU) incorporation, compared to those from control littermates (Fig. 1h, i). BM chimera experiments confirmed an increased proliferation of donor-derived *Sel1l*^{Mx1}-KO HSCs as compared with that of competitor wild-type (WT) HSCs in the same BM (Extended Data Fig. 4m, n), indicating that the increased proliferation of *Sel1l*-deficient HSCs is due to cell intrinsic defect. Detection of long-lived quiescent HSCs with a BrdU label-retention assay showed that BrdU labeling decreased much faster in *Sel1l*^{Vav}-KO HSCs compared to control littermates (Fig. 1j, k). In contrast, we did not observe differences in lineage-negative BM cells (Fig. 1f–k). These data suggest that *Sel1l* loss caused an increase in HSC division with a concomitant loss of quiescence. *Sel1l*-deficiency did not induce apoptosis or mitogen-activated protein kinase (MAPK) signaling that drives ER-stress induced cell death[8] in *Sel1l*^{Mx1}-KO or *Sel1l*^{Vav}-KO HSCs (Extended Data Fig. 4o–t). Collectively, these data demonstrate that SEL1L is required for the maintenance of HSC quiescence.

To understand the impact of SEL1L on HSC competitiveness under hematological stress, we transplanted whole bone marrow (WBM) cells, purified SLAM HSCs or LT-HSCs obtained from *Sel1l*$^{flox/flox}$ or *Sel1l*^{Vav}-KO mice into irradiated recipient mice together with competitor WBM cells. *Sel1l*^{Vav}-KO HSCs completely lost the reconstitution activity (Fig. 2a–c and Extended Data Fig. 5). No donor-derived *Sel1l*^{Vav}-KO HSCs were detected in the BM of recipient mice. Furthermore, we allowed the untreated control or *Sel1l*^{Mx1} donor WBM cells to stably engraft in irradiated recipient mice for 4 weeks before injection of poly(I:C) (Fig. 2d). Deletion of *Sel1l* in reconstituted recipient mice resulted in rapid and almost complete loss of HSC competitiveness (Fig. 2e). Very few donor-derived *Sel1l*^{Mx1}-KO HSCs were recovered from the BM of recipient mice (Fig. 2f). These data demonstrate that SEL1L is essential for the competitiveness of HSCs under hematological stress.

In response to myeloablation agent 5-fluorouracil (5-FU), HSCs begin to proliferate, reach maximal proliferation on day 5–7, and then gradually return to quiescence[9]. *Sel1l* deletion significantly impaired the ability of HSCs to re-enter quiescence after proliferation and resulted in HSC exhaustion 15 days after 5-FU treatment (Fig. 2g, h). We did not observe increased HSC mobilization or apoptosis in the *Sel1l*-deficient HSCs (Fig. 2i and Extended Data Fig. 5f). Challenging the mice with three doses of 5-FU[9] showed that the *Sel1l*-KO mice succumbed much faster than controls and did not survive 5-FU-mediated myeloablation (Fig. 2j). These data demonstrate that loss of SEL1L impairs the re-entry of HSCs into quiescence after proliferation, eventually leading to HSC exhaustion and failure to re-establish homeostasis following hematological stress.

We next investigated how SEL1L regulates HSC identity. First, we asked whether loss of SEL1L induces ER stress and the unfolded protein response (UPR) that may contribute to the impairment of HSCs[10–12]. Transmission electron microscope analysis and quantification

of ER mass showed mild ER stress in $Sell^{Vav}$-KO HSCs as compared to control cells (Extended Data Fig. 6a, b). ER stress triggers UPR that is mediated by IRE1α, ATF6, and PERK[13]. Consistent with an earlier study showing that IRE1α is an ERAD substrate[14], we observed a significant increase in IRE1α protein levels and splicing of its substrate $Xbp1$ ($Xbp1s$) in $Sell$-KO HSCs (Extended Data Fig. 6c, d). PERK and ATF6 pathways were minimally or modestly induced upon $Sell$ deletion (Extended Data Fig. 6c, d). $Sell$-deficiency in certain cell types also induces very mild ER stress, as a result of adaptation through enhanced ER-chaperone expression and UPR activation[15]. Accordingly, we observed a marked upregulation of the ER-chaperones in $Sell$-KO HSCs (Extended Data Fig. 6d). These data suggest that $Sell$ deletion triggers mild ER stress and preferentially induces the IRE1α/XBP1 branch of UPR in HSCs.

To understand whether the $Sell$ loss-induced mild ER stress leads to the loss of HSC identity, we used chemical chaperones tauroursodeoxycholic acid (TUDCA) and 4-phenylbutyric acid (4-PBA)[16], which enhance protein folding and alleviate ER stress (Extended Data Fig. 6e, f, j), to perform the rescue experiments. TUDCA and 4-PBA failed to rescue the steady-state HSCs and the defective reconstitution ability of $Sell$-deficient HSCs (Extended Data Fig. 6g–l). Moreover, chronic levels of ER stress induced by low doses of tunicamycin or thapsigargin did not cause phenotypes in HSCs similar to $Sell$ deletion (Extended Data Fig. 7a–c). These data demonstrate that the $Sell$-KO HSC defects are not attributable to ER stress.

Next, we evaluated the contribution of the upregulated IRE1α/XBP1 pathway to the $Sell$-KO phenotypes by generating $Sell^{flox/flox}$/$Ire1a^{flox/flox}$/Vav-icre and $Sell^{flox/flox}$/$Xbp1^{flox/flox}$/Vav-icre double-KO mice. The combined deletion of $Sell$ and $Ire1a$ or $Xbp1$ led to a more severe HSC deficiency than $Sell$-KO alone (Extended Data Fig. 7d, e). Haploinsufficiency of $Ire1a$ in the $Sell$-KO mice also failed to rescue the phenotype. In contrast to $Sell$-KO mice, loss of $Ire1a$ or $Xbp1$ alone had no effect on HSCs (Extended Data Fig. 7d, e). Moreover, genetic and pharmacological approaches that modulate all UPR pathways or MAPK signaling, including $Xbp1s$ overexpression, IRE1α inhibitor MKC8866, PERK inhibitor GSK2656157, eIF2α inhibitor ISRIB, $Atf6$ knockdown, p38 inhibitor SB202190, ERK inhibitor SCH772984 or JNK inhibitor SP600125[8, 17, 18], were unable to rescue the loss of donor-derived HSCs and defective donor chimerism upon $Sell$ deletion in BM transplantation assays (Extended Data Fig. 7f–r and 8). Collectively, these data demonstrate that the IRE1α/XBP1 pathway provides a protective mechanism to maintain ER homeostasis and prevent HSCs from further damage and the deleterious consequences elicited by $Sell$ deletion. The $Sell$ KO phenotypes are specific to ERAD and independent of ER stress or UPR.

The HSC niche is a key determinant of quiescence and self-renewal[5, 19]. Communication between HSC and niche is mediated by surface receptors and secreted proteins that are synthesized and mature in the ER[4, 20]. We investigated whether $Sell$ deletion compromises the post-translational maturation of the surface receptors in HSCs and thus impairs the HSC-niche interactions. Control or $Sell^{Vav}$-KO HSCs were stained with carboxyfluorescein succinimidyl ester (CFSE) and infused into the irradiated recipient mice. $Sell$-deficient HSCs were located significantly farther from the vascular cells compared to control HSCs

(Extended Data Fig. 9a–c and Supplementary Video 1, 2). Whole-mount imaging of steady-state HSCs[21, 22] in control or *Sel1l*^Vav^-KO mice confirmed the displacement of *Sel1l*-KO HSCs in the BM (Fig. 3a, b).

We next tested whether the mislocalization of *Sel1l*-KO HSCs in the BM permitted donor-HSC engraftment without irradiation. Whereas WT donor cells failed to engraft and reconstitute the non-irradiated control recipient mice, the *Sel1l*^Vav^-KO recipient mice allowed highly efficient donor-HSCs engraftment and reconstitution (Fig. 3c–e). As control, donor-HSCs equally reconstituted the irradiated control or *Sel1l*^Vav^-KO mice (Fig. 3f, g), suggesting that the acceptance of donor engraftment was not due to niche cell defects. Similar nonconditioned transplantation when HSC numbers were comparable in control and *Sel1l*^Mx1^-KO mice showed that only *Sel1l*^Mx1^-KO recipient mice permitted long-term HSC reconstitution (Extended Data Fig. 9d–f). These data demonstrate that *Sel1l*-deficient HSCs are lodged outside the BM niche.

MPL and c-Kit are two master regulators of HSC quiescence and govern interaction with the niche[5]. Deletion of *Sel1l* resulted in a substantial reduction of MPL, but not c-Kit, on the surface of HSCs (Fig. 4a and Extended Data Fig. 9g–j). We also observed a marked decrease of MPL downstream phospho-STAT5 and *p57* expression in *Sel1l*-deficient HSCs (Extended Data Fig. 9k, l). These data demonstrate that SEL1L is essential for surface expression of MPL and its downstream signaling. Reciprocal co-immunoprecipitation experiments showed an interaction between MPL and the ERAD factors SEL1L and HRD1 (Fig. 4b, c). Additionally, MPL was polyubiquitylated by the E3 ligase HRD1(Fig. 4d). Cycloheximide chase assays showed substantial blockade of MPL protein degradation in the absence of SEL1L (Fig. 4e). We confirmed the accumulation of total MPL protein in primary *Sel1l*-KO HSCs (Extended Data Fig. 9m, n). However, MPL was largely co-localized with ER-exclusive chaperone GRP94 and accumulated in the ER in *Sel1l*-KO HSCs (Fig. 4f). These data identify MPL as a bona-fide endogenous substrate of SEL1L-HRD1 and demonstrate that SEL1L deficiency results in profound ER retention of MPL.

We hypothesized that the inability to clear misfolded MPL in the absence of SEL1L causes MPL to be recruited into the misfolded protein aggregates and thus retained in the ER. To test this hypothesis, we used a disease-associated recurrent MPL mutation (R257C) that is predicted to be misfolded and drives the pathogenesis of human congenital amegakaryocytic thrombocytopenia[23] (Extended Data Fig. 9o). The heterozygous arginine-to-cysteine mutation of MPL leads to complete loss of WT-MPL surface expression in patients and causes HSC defects[23]. Most of the MPL-mutant was in the partially glycosylated inmature form in 293T cells and formed high-molecular-weight (HMW) aggregates via disulfide-bonds (Fig. 4g). In contrast, the WT-MPL predominantly formed monomers and was in fully-glycosylated mature form. Importantly, the presence of the misfolded MPL-mutant led to the recruitment of coexpressed WT-MPL into the HMW complexes and formed aggregates while their mRNA levels were comparable (Fig. 4g and Extended Data Fig. 9p). WT-MPL formed HMW aggregates in *SEL1L*-KO, but not in control 293T cells (Fig. 4h). Surface MPL expression was markedly reduced in *SEL1L*- or *HRD1*-KO 293T cells (Extended Data Fig. 9q–x). We confirmed the accumulation of HMW MPL aggregates in primary *Sel1l*-deficient HSCs (Extended Data Fig. 9m). These data indicate that SEL1L-

HRD1 ERAD prevents the dominant-negative effect of misfolded MPL in forming aggregates with the other fraction of MPL that leads to ER retention.

We next asked whether reduced surface expression of MPL causes the mislocalization of *Sel1l*-deficient HSCs in the niche. Similar to *Sel1l*-KO HSCs, steady-state $Mpl^{-/-}$ HSCs are located at a greater distance from the BM vasculature as compared with littermate control (Fig. 4i and Extended Data Fig. 10a). Transplanting equal numbers of CFSE-labeled control or $Mpl^{-/-}$ HSCs into the irradiated recipient mice confirmed the mislocalization of $Mpl^{-/-}$ HSCs in the BM (Extended Data Fig. 10b–d). Blocking the MPL-TPO interaction with MPL- or TPO- neutralizing antibody also led to a significant mislocalization of HSCs in the BM (Extended Data Fig. 10e–i). In contrast, chemical ER stressors did not alter the localization of HSCs (Extended Data Fig. 10j, k). These results demonstrate that MPL is important for HSCs localization in the BM, and that reduced surface MPL is associated with the mislocalization of *Sel1l*-KO HSCs in the niche.

Next, we performed rescue experiments using a MPL agonist that alters the positioning of the MPL dimer to constitutively activate downstream signaling and slows down MPL internalization[24, 25] (Extended Data Fig. 10l). Treatment of $Sel1l^{Mx1}$-KO mice with the agonist successfully restored the phospho-STAT5 levels, and partially rescued the steady-state HSCs (Fig. 5a–c). Furthermore, the MPL agonist partially restored the reconstitution capacity of $Sel1l^{Mx1}$-KO HSCs and the donor-derived $Sel1l^{Mx1}$-KO HSCs in the BM of recipient mice, although the rescue efficiency declined over time (Fig. 5d–f). The rescue effects of MPL agonists depend on the abundance of remaining transmembrane-MPL in *Sel1l*-KO HSCs. However, we observed a time-dependent decrease of surface MPL in *Sel1l*-KO HSCs over the course of reconstitution and in steady-state (Fig. 4a, 5g). This is likely due to the sustained accumulation of misfolded MPL over time, especially when HSCs divide with increased protein synthesis. Although proliferation may dilute out misfoded proteins, recent study shows that increased protein synthesis causes HSCs to accumulate misfolded/unfolded proteins despite of cell proliferation[26]. These data demonstrate that the restoration of MPL signaling with the MPL agonist partially rescues *Sel1l*-deficient HSC phenotypes, but that the rescue is transient until MPL is too low or undetectable on the surface of *Sel1l*-KO HSCs. Besides MPL, it is likely that ERAD also regulates other surface receptors that contribute to HSC maintenance. Future technical advances in the development of highly sensitive proteomic approaches to profile rare population of cells will be required to globally map the ERAD-regulated receptor repertoires in HSCs.

In summary, this study demonstrates an unprecedented physiological mechanism of ER protein quality control machinery in selective regulation of HSC-niche communication and HSC identity (Extended Data Fig. 10m). HSCs exhibit low levels of protein synthesis[27] and employ highly robust protein quality control via ERAD to prevent misfolded protein aggregation and ensure efficient maturation of surface receptors to ultimately safeguard the stem cell pool. Our study reveals an essential stem cell safeguard mechanism that could be potentially targeted to enhance HSC function in future studies.

METHODS

Mice.

Mice were maintained in a pure C57BL/6 background and were kept under specific-pathogen-free conditions in the transgenic mouse facility of Baylor College of Medicine (BCM) (22–24 °C, 30%–70% humidity with 12h dark/12h light cycle). $Sel1l^{flox/flox}$, $Ire1a^{flox/flox}$, $Xbp1^{flox/flox}$ and $Mpl^{-/-}$ mice were described previously[28–31]. The *floxed* mice were crossed with either *Mx1-Cre* (The Jackson Laboratory, 005673) or *Vav-iCre* (The Jackson Laboratory, 008610) mice to generate $Sel1l^{flox/flox}$:*Mx1-Cre*, $Sel1l^{flox/flox}$:*Vav-iCre*, $Ire1a^{flox/flox}$:*Vav-iCre*, or $Xbp1^{flox/flox}$:*Vav-iCre* mice. The $Sel1l^{flox/flox}$:$Ire1a^{flox/flox}$:*Vav-iCre* and $Sel1l^{flox/flox}$:$Xbp1^{flox/flox}$:*Vav-iCre* mice were generated by crossing $Sel1l^{flox/flox}$:*Vav-iCre* mice with $Ire1a^{flox/flox}$ or $Xbp1^{flox/flox}$ mice respectively. 8-week-old $Sel1l^{flox/flox}$:*Mx1-Cre* mice were intraperitoneally injected with poly(I:C) (GE) every other day (1 μg/g body weight) for three times. Poly(I:C)-injected $Sel1l^{flox/flox}$ littermates were used as controls. Both male and female mice were used. For transplantation assays, female eight-to-twelve-week-old C57BL/6-Ly5.1 (CD45.1+) mice (Charles river, 564) were used. All procedures were approved by the BCM Institutional Animal Care and Use Committee. The study is compliant with all relevant ethical regulations regarding animal research.

In vivo assays.

For competitive bone marrow transplantation (BMT) experiments, CD45.1+ recipient mice were lethally irradiated (10 Gy, delivered with 2 equal doses by 4 h apart) and injected retro-orbitally with either 250 freshly sorted CD45.2+ HSCs, together with 250,000 helper CD45.1+ BM cells, or CD45.2+ BM cells with equal numbers of CD45.1+ competitor BM cells. For genetic rescue experiments, 2,000 sorted Zsgreen/GFP+ HSPCs were transplanted into lethally irradiated CD45.1+ recipient mice together with 250,000 CD45.1+ BM cells. For non-conditioned transplantation experiments, recipient mice were injected with 1×10^7 CD45.1+ BM cells via tail vein. To induce *Sel1l* deletion after the donor cells stably engraft in the recipient mice, irradiated recipient mice were injected with polyI:C 4 weeks after transplantation and were analyzed for donor-derived chimerism at indicated time points. For HSCs localization assay, 10,000 CFSE labelled HSCs were injected retro-orbitally to lethally irradiated mice 24h before analysis. Mice were injected intraperitoneally with 5-fluorouracil (Sigma, F6627) (150 mg/kg) once or 3 times at 11 days interval. For BrdU incorporation assay, mice were injected intraperitoneally with one dose of BrdU (Sigma, B5002; 1 mg/6g body weight) 12h prior to euthanization. For pulse-chase assay, mice were injected with one dose of BrdU as above and were maintained on 1mg/ml BrdU in drinking water for 10 days, followed by regular water feeding for up to 42 days. Amber bottles containing BrdU were changed every 3 days. For rescue experiments, MPL agonist was dissolved in DMSO (40 mg/ml) and resuspended in 1% microcrystalline cellulose and 50% sucrose solution and was administered by daily oral gavage (2mg/kg). For treatment under BMT condition, PBMCs from three randomly picked control or $Sel1l^{Mx1}$ donors were collected before treatment to examine donor chimerism. Mice from the same batch BMT experiment were then randomized for treatment. The PERK inhibitor GSK2656157 was formulated in 0.5% hydroxypropyl methyl cellulose, 0.1% tween-80 in water (pH 6.75) and was administered by daily oral gavage (150 mg/kg). The IRE1α RNase inhibitor MKC8866

was formulated in 1% microcrystalline cellulose and 50% sucrose solution and was administered by daily oral gavage (150 mg/kg). The eIF2α inhibitor ISRIB (2.5 mg/kg, every two days), p38 inhibitor SB202190 (20 mg/kg, daily), ERK inhibitor SCH772984 (25 mg/kg, daily) and JNK inhibitor SP600125 (20 mg/kg, daily) formulated in 45% saline, 50% PEG 400, 5% DMSO was administered by intraperitoneal injection. Tunicamycin or thapsigargin was administrated at 0.1 mg/kg (three times/week) by intraperitoneal injection (150 mM dextrose, 1% DMSO in PBS). Tauroursodeoxycholic acid (TUDCA) was administered daily by intraperitoneal injection (200 or 500 mg/kg in PBS). Mice were given regular drinking water or 4-PBA (1 g/kg/day) in the drinking water. For TPO-MPL neutralization assay, mice were administered daily by intraperitoneal injection of 5mg/kg of anti-TPO (Biolegend, # 696104), anti-MPL antibody (Biolegend, #393702) or isotype control antibodies (Biolegend, # 400602 and #401502) respectively. For survival assay, Mice were euthanized when endpoints were met according to approved IACUC protocol. The information of chemicals are in Supplementary Table 1.

Retroviral HSPCs transduction assays:

Retrovirus was generated in 293T cells. LSK cells sorted from 8-week-old control or $Sel1l^{Mx1}$ mice were cultured in X-Vivo 15 medium (Lonza, 04–418Q) supplemented with 1% heat-inactivated FBS, 50 ng/ml SCF, 50 ng/ml TPO, 10 ng/ml IL-3 and 10 ng/ml IL-6 (Peprotech) for 24 hours. Cells were spin-infected with retroviral supernatant supplemented with polybrene (8 mg/ml) in retronectin (Clontech, T202) coated plates at 1,100g for 90 min at 32 °C. Fresh medium was replaced 3 hours after spin-infection. Cells were spin-infected again on the 3rd day. GFP/Zsgreen+ cells were sorted for BMT assay on the 4th day.

Colony forming unit (CFU) assay.

For CFU assay, freshly purified HSCs were plated in methylcellulose culture medium (Stem Cell Technologies, M3434). BFU-E, CFU-GM/G/M, CFU-GEMM were scored on day 12 under an inverted microscope and standard morphological criteria[32].

Flow cytometry and cell sorting.

Flow cytometry data were collected by BD FACS Diva 8 on BD LSR II or BD Fortessa analyzer. Cell sorting experiments were performed on FACS Aria II cell sorter (BD). The acquired data were analyzed using FlowJo 10 software. BM cells were isolated by flushing the femur/tibia with Ca^{2+}- and Mg^{2+}-free DPBS containing 2% FBS using a 10 ml syringe fitted with a 25-gauge needle. Spleen cells were obtained by gently crushing the spleen. Peripheral blood was obtained via tail vein bleeding. Complete blood count analyses were performed using a Hemavet haematology system (Drew Scientific). Erythrocytes were removed by ACK lysis buffer (Thermo Fisher, A1049201). Single-cell suspensions of BM cells, spleen cells or PBMCs were obtained by filtering through 40 μm strainers. For cell analyses, BM cells or spleen cells were incubated with anti-mouse Lineage Cocktail (including CD3 (17A2), Gr-1 (RB6-8C5), CD11b (M1/70), B220 (RA3-6B2) and Ter119) , c-Kit (2B8), Sca-1 (E13-161.7), CD150 (TC15-12F12.2), and CD48 (HM48-1) for SLAM HSCs; or together with c-Kit (2B8), Sca-1 (E13-161.7), CD34 (RAM34), and Flk2 (A2F10) for LT-HSCs; or together with c-Kit (2B8), Sca-1 (E13-161.7), FcγR (93), CD34 (RAM34), Flk2 (A2F10), and IL7Rα (A7R34) for progenitors. CD3 (17A2), Gr-1 (RB6-8C5), CD11b

(M1/70), and B220 (RA3-6B2) were used for analyses of mature cells in peripherial blood. CD45.1 (A20) and CD45.2 (104) antibodies were used for analyses of donor chimerism in the transplantation assay. Anti-MPL (S16017E) antibody was used to evaluate MPL protein expression on HSCs. Antibodies were obtained from Biolegend or eBioscience (Supplementary Table 2). DAPI was used to exclude dead cells.

For cell sorting, single cells were incubated with the lineage depletion beads (Miltenyi, 130-110-470) followed by LS column depletion (Miltenyi,130-042-401). The lineage-depleted fraction was used for staining as described above.

For intracellular Ki67 staining, lineage-depleted BM cells were fixed and permeabilized with True-Nuclear™ transcription factor buffer (Biolegend, #424401) after surface maker staining. Then cells were stained with anti-Ki-67 antibody (BioLegend, # 652405) for 1 hour at room temperature (RT). Cells were resuspended in flow buffer containing 1 μg/mL DAPI for analysis. Lineage-depleted BM cells were stained with surface markers to define each BM subset followed by intracellular staining using the BrdU staining kit according to the manufacturer's instructions (BD Biosciences). For Annexin V staining, lineage-depleted BM cells were firstly stained with surface makers and then stained with Annexin V antibody for 30 mins at RT in Annexin V binding buffer (eBioscience, 88-8007-72). Cells were resuspended in flow buffer with 1 μg/mL DAPI for analysis. For intracellular phosphoprotein staining, sorted SLAM HSCs were fixed by IC Fixation Buffer (eBioscience, # 00-8222-49) for 30 mins at RT followed by permeabilization with methanol for 1 hour at 4°C. Cells were then stained by indicated antibodies (Supplementary Table 1). For ER analyses, sorted SLAM HSCs were washed with HBSS, incubated for 15 min at 37°C with 100 nM ER-Tracker Green (Thermo Fisher, E34251) in HBSS containing 50 μM verapamil (Sigma, V4629). Cells were then washed and resuspended with HBSS containing 50 μM verapamil for flow analysis.

Immunofluorescence staining.

SLAM HSCs were sorted as above in PBS and fixed with 4% PFA for 10 min at RT. Cells were then applied onto poly-lysine coated slides by cytospin, permeabilized in PBS containing 0.1% Triton X-100 for 5 min and blocked in PBS containing 1% BSA for 1h at RT. Slides were then incubated with either anti-GRP94 (Cell Signaling, #20292), anti-MPL (Biolegend, S16017E), Normal Rabbit IgG (Cell Signaling, #2729), or Purified Mouse IgG2a, κ Isotype Ctrl Antibody (Biolegend, 401501) in PBS containing 1% BSA for 12h at 4 °C. Slides were then washed three times in PBS containing 0.05% Tween-20 and incubated with Alexa Fluor 488-conjugated goat anti-mouse IgG (Invitrogen, A-11029), or Alexa Fluor 594 -conjugated goat anti-rabbit IgG (A-11012) secondary antibody in PBS containing 1% BSA in dark for 1h at 37°C. Slides were washed three times in PBS with 0.05% Tween-20 and mounted using VectaShield (Vector Laboratories) containing 1 μg/ml DAPI. Immunofluorescent images were acquired on GE Healthcare DeltaVision LIVE Deconvolution Microscope (20x air or 100x oil) along the z axis (step size 0.25 μm). Images obtained by 20x objective were processed and analyzed by CellProfiler 3.0 to quantify the expression of GRP94 protein and MPL protein in HSCs. Images obtained by 100x objective were processed and analyzed by BioImageXD 1.22[33] to quantify the co-localization

(Mander's coefficient) between GRP94 signals and MPL signals. The representative images of control or *Sel1l*-KO HSCs were presented in the same scales using ImageJ 1.51.

For immunofluorescence staining of frozen sections of long bones, recipient mice were perfusion-fixed and the bones were post-fixed for 4 hours with 4% PFA at 4°C. The bones were embedded, and sectioned (60μm) according to the Kusumbe method[34]. Sections were rehydrated and permeabilized in PBS with 0.3% Triton X-100, and blocked in staining solution (PBS containing 5% Donkey serum, 10% DMSO, 0.5% IgePal-CA630) plus anti-mouse CD16/32 antibody (1:100, 70-0161-M001, Tonbo Bio) for 4 hours. Sections were then stained overnight with anti-CD150-PE (Biolegend, 400213, 1:100), Biotin lineage cocktail (Supplementary Table 1), anti-CD31 (R&D, AF3628, 1:200), anti-VE-Cadherin (R&D, AF1002, 1:200) in staining at 4°C. Donkey anti-goat Alexa Fluor 647 (1:200, 705-606-147, Jackson Immunoresearch) and Alexa Fluor 488-streptavidin (Biolegend, 115918, 1:100) were used as secondary antibodies for overnight incubation in staining solution at 4°C. Slides were mounted with anti-fade prolong diamond (P36961, Thermo Fisher), and imaged immediately by a Zeiss LSM780 confocal microscope with a 20x objective. Z-stack images were acquired at 1 μm steps in 16-bit greyscale. The stacks were converted into RGB images, and the noise was removed from the images by the despeckle function of ImageJ 1.51. A threshold was given to reduce the background in each channel. 3D images and videos were produced by the 3D viewer plugins in ImageJ 1.51. The distance from HSCs to the closest vessel was measured with ImageJ 1.51.

Transmission Electron Microscopy.

Around 20,000 freshly sorted control or *Sel1l*[Vav]-KO SLAM HSCs were fixed (3% PFA, 2.5% glutaraldehyde and 0.1 M cacodylate) in 1.5 ml microcentrifuge tubes for 1 hour at room temperature. Fixed HSCs were washed once by 0.1M cacodylate buffer (CB) and stained by Evans blue (1 mg/ml in 0.1M CB) for 20 minutes at room temperature. HSCs were washed 3 times by 0.1M CB and pelleted in 2% low melting agarose[35]. Solidified agarose with HSCs pellet was trimmed and washed in 0.1M CB and treated with 0.1% Millipore-filtered cacodylate buffered tannic acid, post fixed with 1% buffered osmium, and stained with 1% Millipore-filtered uranyl acetate. The samples were dehydrated in increasing concentrations of ethanol, infiltrated, and embedded in LX-112 medium. The samples were polymerized in a 60°C oven for approximately 3 days. Ultrathin sections were cut in a Leica Ultracut microtome (Leica), stained with uranyl acetate and lead citrate in a Leica EM Stainer, and examined in a JEM 1010 transmission electron microscope (JEOL) at an accelerating voltage of 80 kV. Digital images were obtained using AMT Imaging System (Advanced Microscopy Techniques Corp).

Quantitative real-time PCR

Cells were sorted directly into TRIzol LS Reagent (Invitrogen, #10296010). Total RNA was extracted according to the manufacturer's instructions. Total RNA was reverse transcribed using SuperScript IV Reverse Transcriptase (Invitrogen, 18091050). Quantitative real-time PCR was performed using SYBR Green PCR master mix (Applied Biosystems, 4367695) on a QuantStudio 6 Real-Time PCR system (Applied Biosystems). Primer sequences are in Supplementary Table 3.

Plasmids.

The following plasmids were used: The pMSCV-*Xbp1s*-IRES-*GFP* plasmid was generated by cloning the *Xbp1s* cDNA into pMSCV-IRES-*GFP* (pMIG, Addgene, #20672); The LEPZ miR30-based control shRNA that targets Renilla Luciferase (shRen.713) was a gift from Johannes Zuber (Addgene, # 111161). The oligonucleotides targeting mouse *Atf6* (5'-TGCTGTTGACAGTGAGCGCCAGCAGGTACATACACCTCAATAGTGAAGCCACAGA TGTATTGAGGTGTATGTACCTGCTGATGCCTACTGCCTCGGA-3') was synthesized to generate sh*Atf6* construct as reported[36]; The *MPL, SEL1L* and *HRD1* gene was PCR amplified from mouse BM cDNA and cloned into pcDNA3.1-Myc tag and pcDNA3.1-FLAG tag vectors; The R258C mutated *MPL* and the *HRD1* RING finger mutant (C291A/ C294A) was generated by overhang extension (OE) PCR and cloned into pcDNA3.1-Myc tag and/or pcDNA3.1-FLAG tag vector; The GFP was amplified from pMIG and cloned into pcDNA3.1-Myc tag and pcDNA3.1-FLAG tag vector; pMx-HA-MPL used in Fig. 4h (gift from Wei Tong, University of Pennsylvania, USA); pcDNA3.1-proAVP(G57S)-HA and pcDNA3.1-POMC (C28F)-FLAG (gifts from Ling Qi, University of Michigan, USA). Primers used to generate the plasmids are in Supplementary Table 3.

Co-immunoprecipitation.

293T cells were transfected with plasmids as indicated in Figure 4b, c. Cells were lysed in lysis buffer (1% Triton X - 100, 150 mM NaCl, 1 mM EDTA, 50 mM Tris-HCl pH7.5) supplemented with 1X protease inhibitor cocktail (Roche, 14826500) 36h after transfection. A total of 2mg protein lysates was incubated with antibody-conjugated affinity gel (anti-FLAG M2, Sigma F-2426; or anti-Myc, Sigma E6654) overnight at 4°C with gentle rocking. Immunocomplexes were washed once with lysis buffer followed by three times with wash buffer (1% Triton X-100, 137 mM NaCl, 2 mM EDTA, 20 mM Tris-HCl pH 7.5, 10% glycerol), eluted directly by boiling in 2X SDS sample buffer without DTT (100 mM Tris-HCl pH 6.8, 2% SDS, 0.01% bromophenyl blue, 10% glycerol) for 10 minutes. The samples were spun down at 12,000 g for 1 minute and supernatant was transferred to microcentrifuge tubes containing DTT (0.1 M final concentration). Samples were analyzed by SDS-PAGE and Western blot (WB). Antibodies used are in Supplementary Table 2.

Cycloheximide (CHX) chase assay.

WT or *SEL1L* CRISPR knockout 293T cells[37] were transfected with pcDNA3.1-MPL-Myc tag or pcDNA3.1-MPL mutant-Myc tag plasmid. Cells were treated with CHX (Millipore, 239764, 200 μg/ml) for the indicated times thirty-six hours post-transfection. Cells were lysed in 1x SDS sample buffer (50 mM Tris-HCl pH 6.8, 1% SDS, 0.005% bromophenyl blue, 0.1 M DTT, 5% glycerol) and boiled for 10 minutes followed by SDS-PAGE and WB. Antibodies used are in Supplementary Table 2.

In vivo ubiquitylation assays.

293T cells were transfected with indicated plasmids as in Fig. 4d. 36h post-transfection, cells were treated with 10 μM MG132 for 6h. Cells were lysed in denaturing buffer (1% SDS, 50 mM Tris-HCL, pH 7.5, 0.5 mM EDTA, 10 mM N-ethymaleimide and 1 mM DTT). After incubation at 100°C for 10 minutes, the lysate was sonicated for 5 minutes by

Bioruptor (Diagenode, B01020001) at high amplitude and 30s on/30s off. Supernatant of the lysate was dilute with lysis buffer (1% Triton X-100, 150 mM NaCl, 1 mM EDTA, 50 mM Tris-HCl pH7.5, and 10 mM N-ethymaleimide) supplemented with 1x protease inhibitor cocktail (Roche, 14826500). Immunoprecipitation and western blot were performed as described above. Antibodies used are in Supplementary Table 2.

Non-reducing western blot.

293T cells were transfected with pcDNA3.1-MPL-Myc tag, pcDNA3.1-MPL mutant-Myc tag or pcDNA3.1-MPL-Myc tag together with pcDNA3.1-MPL mutant-Myc tag plasmids. 36h post-transfection, cells were lysed in 1x SDS sample buffer (50 mM Tris-HCl pH 6.8, 0.1% SDS, 0.005% bromophenyl blue, 5% glycerol) without reducing agent and boiled for 10 minutes followed by SDS-PAGE and WB.

Western blot for HSC.

WB was performed as described previously[38]. Approximately 20,000 SLAM HSCs were sorted into 250 µl PBS containing 20% trichoracetic acid (TCA). The concentration of TCA was adjusted to 10% after sorting. Extracts were incubated on ice for 30 min and centrifuged at 13,000 rpm for 10 min at 4°C. Precipitates were washed in pure acetone (Fisher scientific, A18-4) twice and the dried pellets were solubilized in 9 M urea, 2% Triton X-100, and 1% DTT together with 1X LDS buffer (Invitorgen, NP0007). Samples were separated on NuPAGE 4–12% Bis-Tris protein gels (Invitrogen, NP0336BOX) and transferred to PVDF membrane (Millipore). The blots were incubated with primary antibodies overnight at 4°C and then with secondary antibodies. NativePAGE™ 4-16% Bis-Tris protein gel was used to detect MPL aggregates in HSCs as manufacturer's instructions[39] (Invitrogen, BN1002BOX). Blots were developed with the SuperSignal West Femto chemiluminescence kit (Thermo Scientific, 34096). Antibodies and reagents used are in Supplementary Table 1 and 2.

### Statistics and Reproducibility.

Data are expressed as mean ± standard deviation (s.d.), or mean ± standard error of the mean (s.e.m.) as indicated in the figure legend. *n* is the number of independent biological replicates unless indicated specifically in the figure legend. Respective *n* values are shown in the figure captions and in the source data files. Pooled mice were used for Figs 2a, 4f and Extended Data Figs 4b, 5d, 6a, 6c, 9b, 9m, 9n and 10b . Experiments for Figs. 3a–e,4b–e, 4i, 4g and Extended Data Figs 4b, 6c, 9m, 9r and 9u–w were performed at least twice independently. Experiments for Figs. 4h and Extended Data Figs.1a, 7n and 8 were performed once. Mice for transplantation were randomized and no blinding protocol was used. No statistical method was used to predetermine sample size. The results were quantified using GraphPad Prism 7. *P* values were generated using two-tailed unpaired/paired (Extended Data Fig. 9h), Student's t-test, two-sample Kolmogorov–Smirnov test, two-way ANOVA with Bonferroni's multiple comparison test or Fisher's LSD test (Extended Data Fig. 6i, 6l, 7m, 7p, 8b (right panel), 8d (right panel), 8f (right panel)), one-way ANOVA with Tukey's multiple comparison tests or Fisher's LSD test (Fig. 5e) as indicated.

Data availability.

Previously published sequencing data that were re-analysed here are available under accession codes GSE60101 for Fig 1a [7] and GSE109125 for Extended Data Fig 2b [6].

Source data are provided with this study. All other data supporting the findings of this study are available from the corresponding author on reasonable request.

Extended Data
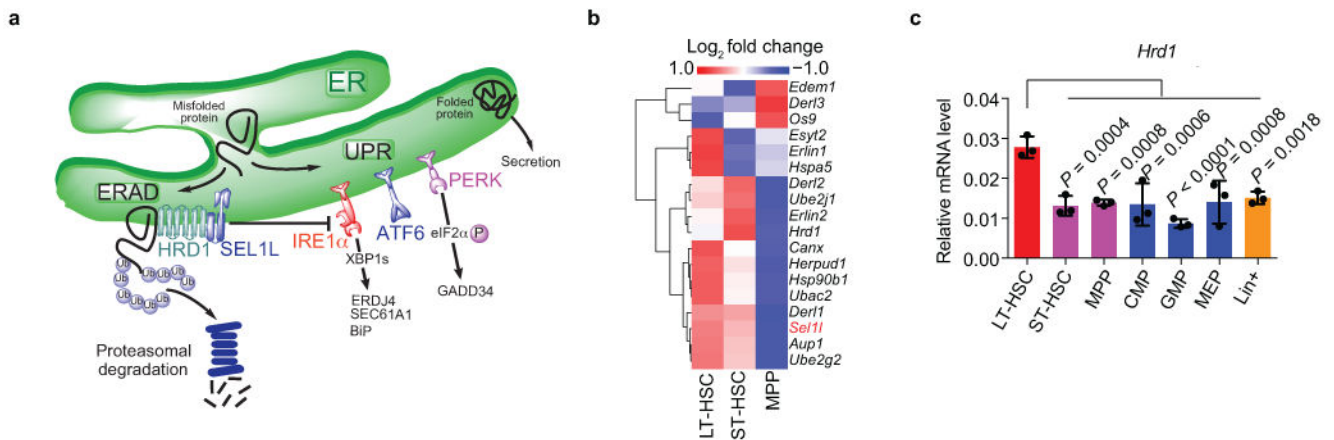
**Extended Data Fig. 1. SEL1L-ERAD is highly expressed in HSCs compared to progenitors**
a, Diagram showing the ERAD and UPR pathways. The ER is the major subcellular site for synthesis and maturation of all transmembrane and secreted proteins. To maintain protein homeostasis and normal cell function, cells have evolved highly sensitive and sophisticated quality control systems and/or stress response pathways to ensure the fidelity of protein structure. Two such systems conserved across different species are ERAD and UPR. Among the mammalian ERAD complexes, the SEL1L-HRD1 complex, consisting of the E3 ubiquitin ligase HRD1 and its adaptor protein SEL1L, is the most conserved branch that ubiquitinates and targets selective substrates for proteasomal degradation. Many physiological or pathological stresses cause the accumulation of unfolded or misfolded proteins in the ER and activate the ER stress response or UPR that is mediated by three ER transmembrane sensors IRE1α, ATF6 and PERK. IRE1α is the most ancient and conserved sensor of the UPR. Upon activation, IRE1α dimerizes and trans-autophosphorylates to activate its RNase domain to induce unconventional splicing of its substrate XBP1. Recent study reveals that IRE1α, rather than ATF6 and PERK, as a selective endogenous substrate that is degraded by SEL1L-HRD1 ERAD. **b**, Heatmap showing the expression of ERAD genes in mouse HSCs and progenitors. LT-HSC: long term HSC (LSK CD150+CD48−CD135−); ST-HSC: short term HSC (LSK CD150−CD48−CD135−); MPP: multipotent progenitors (LSK CD135+). Data extracted from GSE109125. **c**, Quantitative RT–PCR analysis of *Hrd1* expression in mouse HSCs and progenitors. Data are presented relative to *Gapdh*. *n* = 3 biologically independent mice. One-way ANOVA was used to calculate *P* values. Results are shown as mean ± s.d. Statistical information is provided as source data.
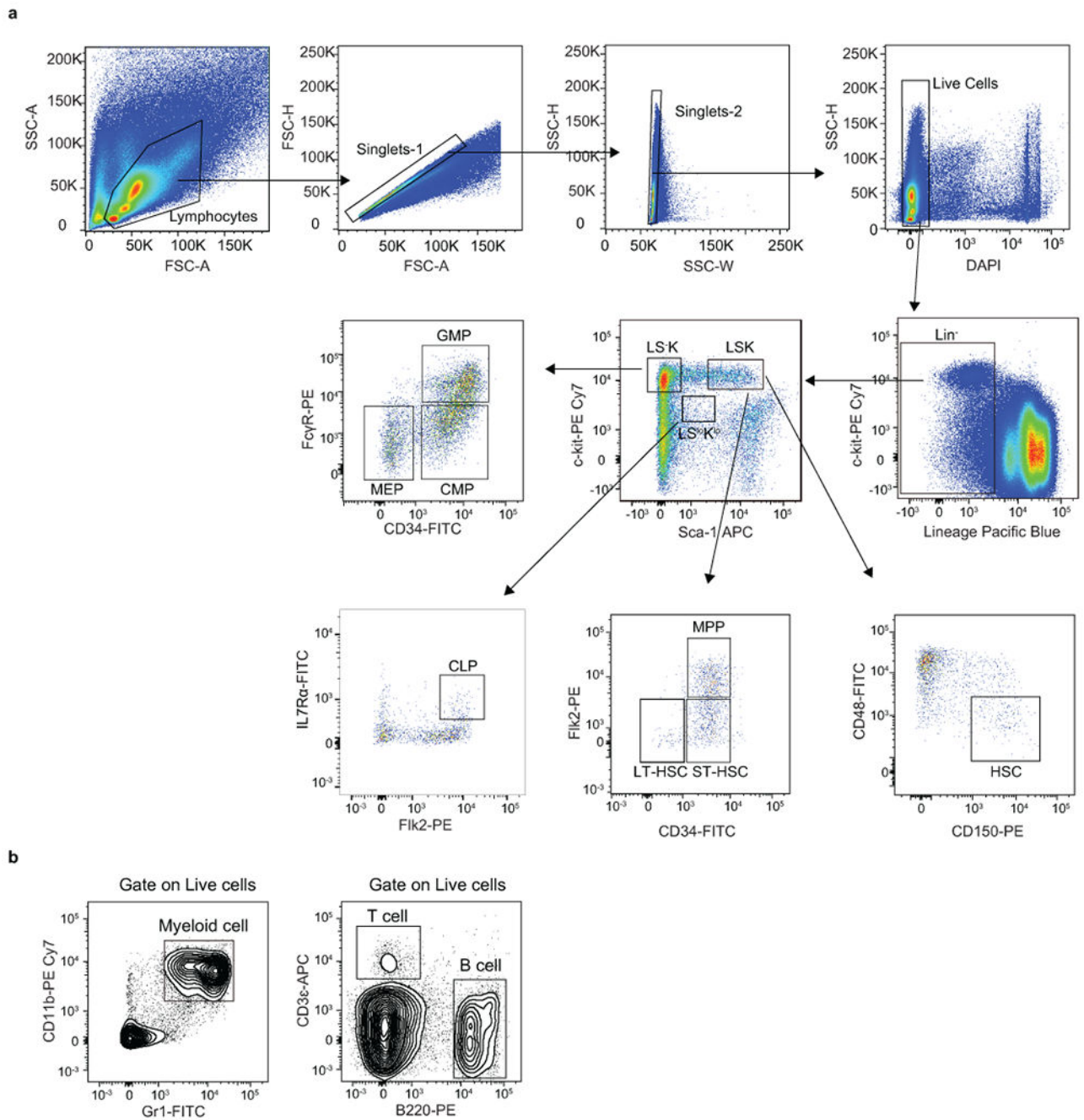
Extended Data Fig. 2. Representative flow cytometry gating strategy used in this study

a, Strategy used to isolate the hematopoietic stem and progenitor cell populations in mouse bone marrow presented on Fig. 1d, 1f, 1h, 1j, 2c, 2f, 2h, 2i, 3e, 3g 4a, 5b, 5c, 5f, 5g, Extended Data Fig. 3c, 3d, 4e, 4g, 4i, 4n–q, 4s, 4t, 5c, 5f, 6b, 6g, 6i, 6l, 7b–e, 7i, 7m, 7p, 7r (right panel), 8a–f (right panel), 9e, 9g, 9k, 10a and 10f. LSK: Lin⁻Sca-1⁺c-Kit⁺; LT-HSC: long-term HSC (LSK CD34⁻Flk2⁻); ST-HSC: short-term HSC (LSK CD34⁺Flk2⁻); MPP: multipotent progenitors (LSK CD34⁺Flk2⁺); CLP: common lymphoid progenitors (Lin⁻Sca-1^{low}c-Kit^{low}Flk2⁺IL7Rα⁺); CMP: common myeloid progenitors (LS-K CD34⁺FcγR

−); GMP: granulocyte/macrophage progenitors (LS-K CD34$^+$ FcγR$^+$); MEP: megakaryocytic/erythroid progenitors (LS-K CD34$^-$FcγR$^-$). **b**, Strategy used to isolate myeloid cell (CD11b$^+$Gr1$^+$), B cell (B220$^+$CD3ε^-) and T cell (CD3ε^+B220$^-$) in mouse bone marrow presented on Fig.2b, 2e, 3d, 5e, Extended Data Fig. 3e, 5b, 5e, 6h, 6k, 7h, 7l, 7o, 7r (left panel), 8b(left panel), 8d (left panel), 8f (left panel) and 9f.
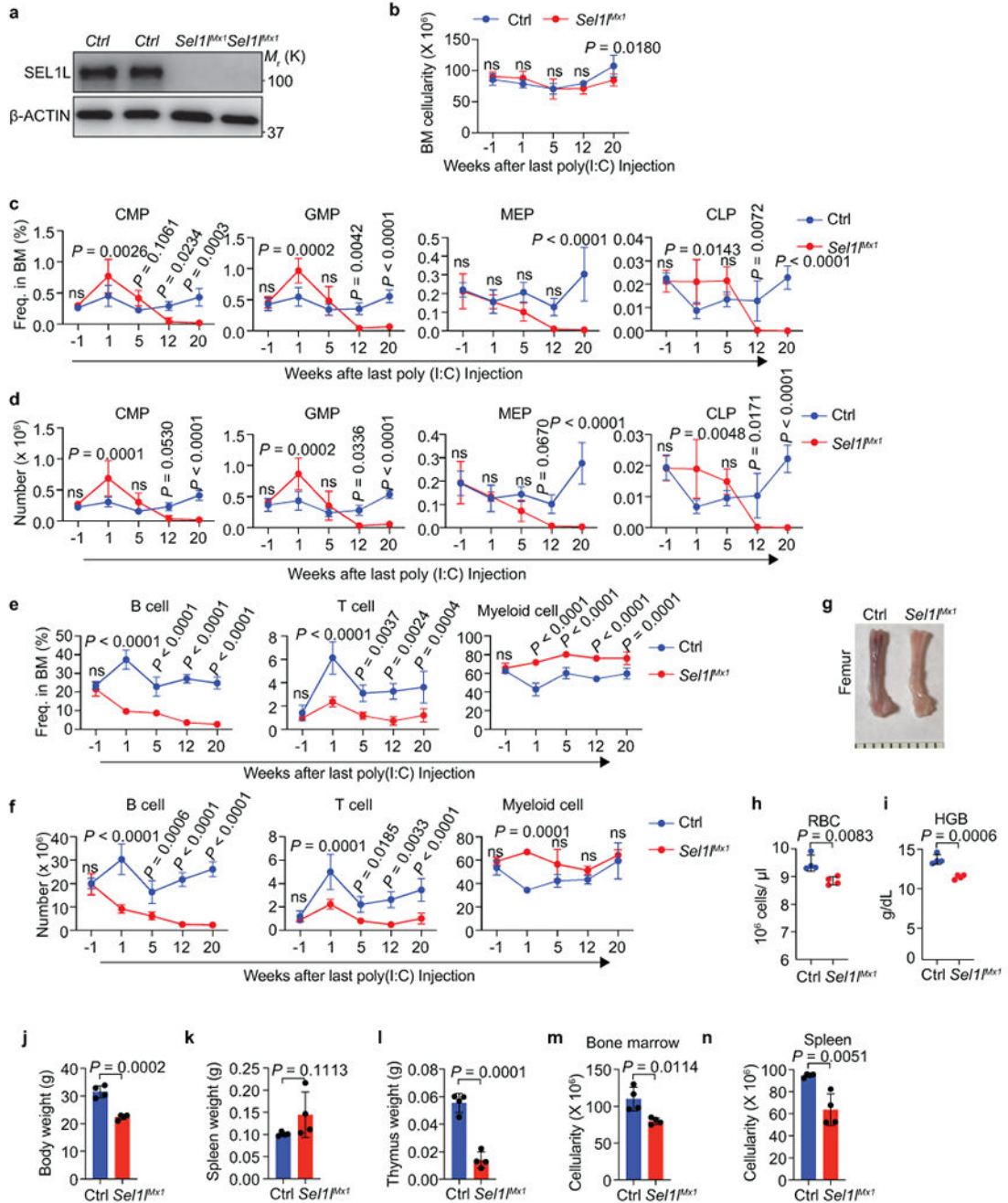
Extended Data Fig. 3. Progressive loss of progenitor cells in *Sel1l* knockout mice

a, Western blot analysis of SEL1L expression in LSK cells from 2 control (Ctrl) and 2 *Sel1l^Mx1* mice 1 week after last poly (I:C) injection. β-ACTIN was used as loading control. **b**, Bone marrow (2 femurs and 2 tibiae) cellularity of Ctrl and *Sel1l^Mx1* mice at the indicated time points. −1 indicates 1 week before poly (I:C) injection. Age and gender matched littermates were used in each time points. Ctrl (12, 20): $n = 5$, Ctrl (5): $n = 6$ and the others: $n = 4$. **c, d**, Percentage (**c**) and number (**d**) of CMP, GMP, MEP and CLP in the BM of control (Ctrl) and *Sel1l^Mx1* mice at the indicated time points. Ctrl (12, 20): $n = 5$, Ctrl (5): $n = 6$ and the others: $n = 4$. **e, f**, Percentage (**e**) and number (**f**) of B, T and myeloid cells in the BM of control (Ctrl) and *Sel1l^Mx1* mice at the indicated time points. Ctrl and *Sel1l^Mx1* (1, 12): $n = 3$, Ctrl (5): $n = 6$ and the others: $n = 4$. **g**, Representative image of femur bone from control and *Sel1l^Mx1* mice 30 weeks after poly (I:C) injection. **h, i**, Quantification of Red blood cell (RBC, **h**) and hemoglobin (HGB, **i**) in peripheral blood of Ctrl and *Sel1l^Mx1* mice 30 weeks after poly (I:C) injection. $n = 4$. **j-l**, Body weight (**j**), spleen weight (**k**) and thymus weight (**l**) in control and *Sel1l^Mx1* mice as in h. $n = 4$. **m, n**, BM (**m**) and spleen (**n**) cellularity in mice as in h. $n = 4$. Results are shown as mean ± s.d. Two-way ANOVA (**b-f**) or two-tailed Student's t-tests (**h-n**) was used to assess statistical significance. ns, not significant. Statistical information and unprocessed blots are provided as source data.
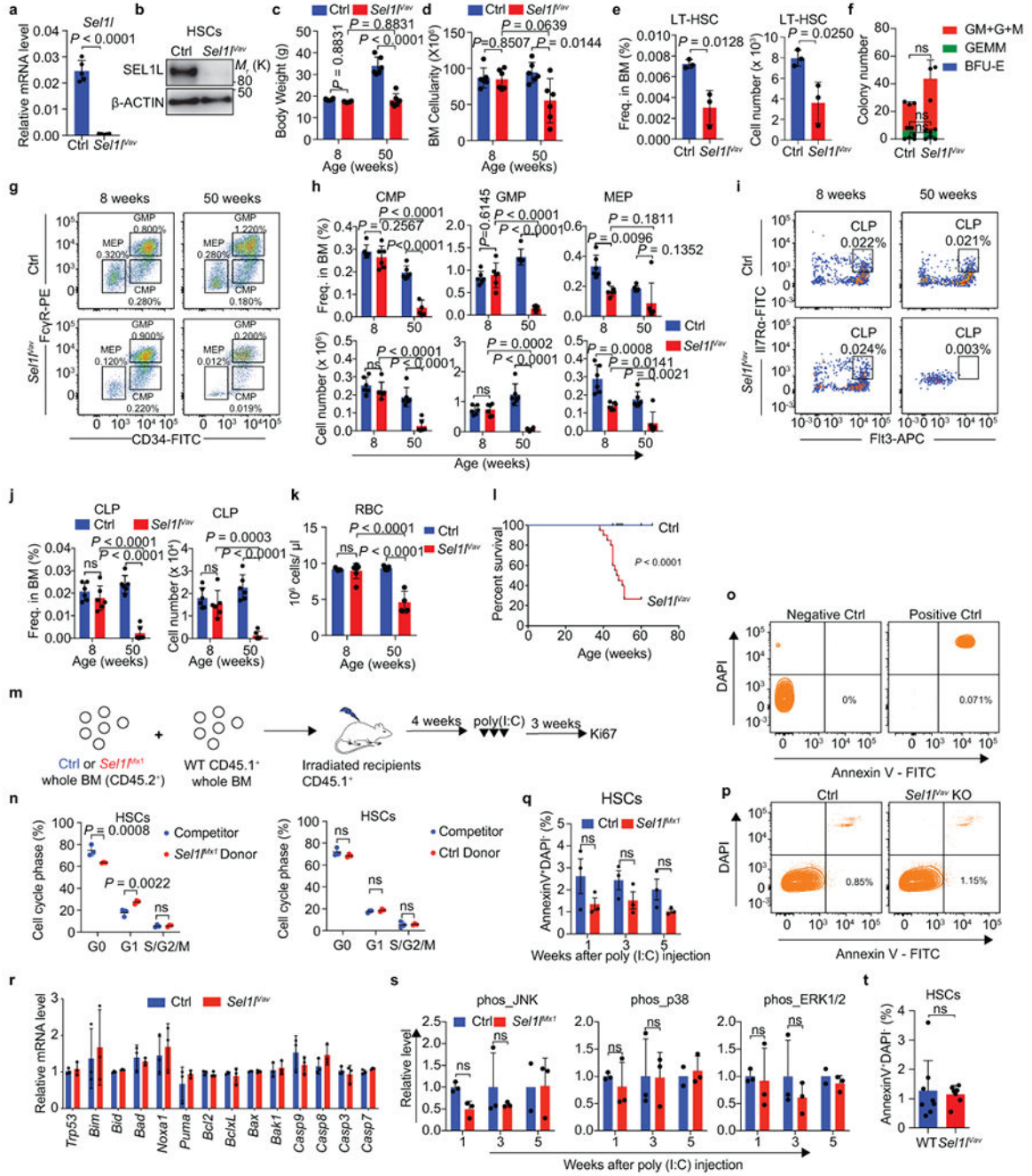
Extended Data Fig. 4. Characterization of the $Sel1l^{Vav}$ knockout mice

a, **b**, Expression of Sel1l mRNA (**a**) or protein (**b**) in primary control (Ctrl) or $Sel1l^{Vav}$-KO HSCs. $n = 5$ in **a**. **c,** Body weight of Ctrl and $Sel1l^{Vav}$-KO mice at indicated time points, $n = 6$. **d**, BM cellularity of Ctrl and $Sel1l^{Vav}$-KO mice at the indicated time points. $n = 6$. **e**, Frequency and absolute number of LT-HSCs from 8-week-old Ctrl and $Sel1l^{Vav}$-KO mice. $n = 3$. **f**, Colony formation in methylcellulose from equal number of Ctrl or $Sel1l^{Vav}$-KO HSCs. CFU-GM/G/M: colony forming unit granulocytic and monocytic (GM)/ granulocytic (G)/ monocytic (M); CFU-GEMM: colony forming unit granulocytic, erythrocytic,

monocytic and megakaryocytic; BFU-E: blast forming unit erythrocytic. The colonies were counted after 12 days of culture. $n = 3$. **g-j**, Representative pseudocolor dot plots showing the gating strategy to identify CMP, GMP, MEP, CLP (**g, i**) and quantification (**h, j**) in the BM of Ctrl and *Sel1l*[Vav]-KO mice. $n = 6$ for each group. **k**, RBC count in peripheral blood of Ctrl and *Sel1l*[Vav]-KO mice at indicated age. 8-week-old Ctrl: $n = 3$; 8-week-old *Sel1l*[Vav]: $n = 7$; 50-week-old Crl: $n = 7$; 50-week-old *Sel1l*[Vav]: $n = 5$. **l**, Kaplan–Meier survival analysis of Ctrl and *Sel1l*[Vav]-KO mice. $n = 20$. **m**, Schematic diagram of the Ki67 assay under BMT condition. **n**, Cell cycle analysis of donor and competitor derived HSCs using Ki67 and 7-AAD. $n = 3$. **o, p**, Representative FACS plot for apoptosis analysis from freshly isolated control and *Sel1l*[Vav]-KO HSCs. Sample without Annexin V stain served as negative control. Sample treated by heat shock served as positive control. **q**, Quantification of apoptotic HSCs in control and *Sel1l*[Mx1]-KO mice at indicated time points, $n = 3$. **r**, Quantification of apoptosis-related genes expression in control and *Sel1l*[Vav]-KO HSCs. $n = 4$. **s**, Quantification of phos-p38, phos-JNK and phos-ERK in control and *Sel1l*[Mx1] HSC at indicated time points. $n = 3$ for all groups except 5 weeks Ctrl ($n = 2$). **t**, Percentage of apoptotic HSCs in the BM of 8-week-old Ctrl and *Sel1l*[Vav]-KO mice. Ctrl: $n = 8$; *Sel1l*[Vav]: $n = 7$. Two-way ANOVA (**c, d, h, j, k, q, s**), two-tailed Student's t-tests (**a, e, f, n, r, t**), or log-rank test (**l**) were used to calculate P values. Results are shown as mean ± s.d. ns, not significant. Statistical information and unprocessed blots are provided as source data.
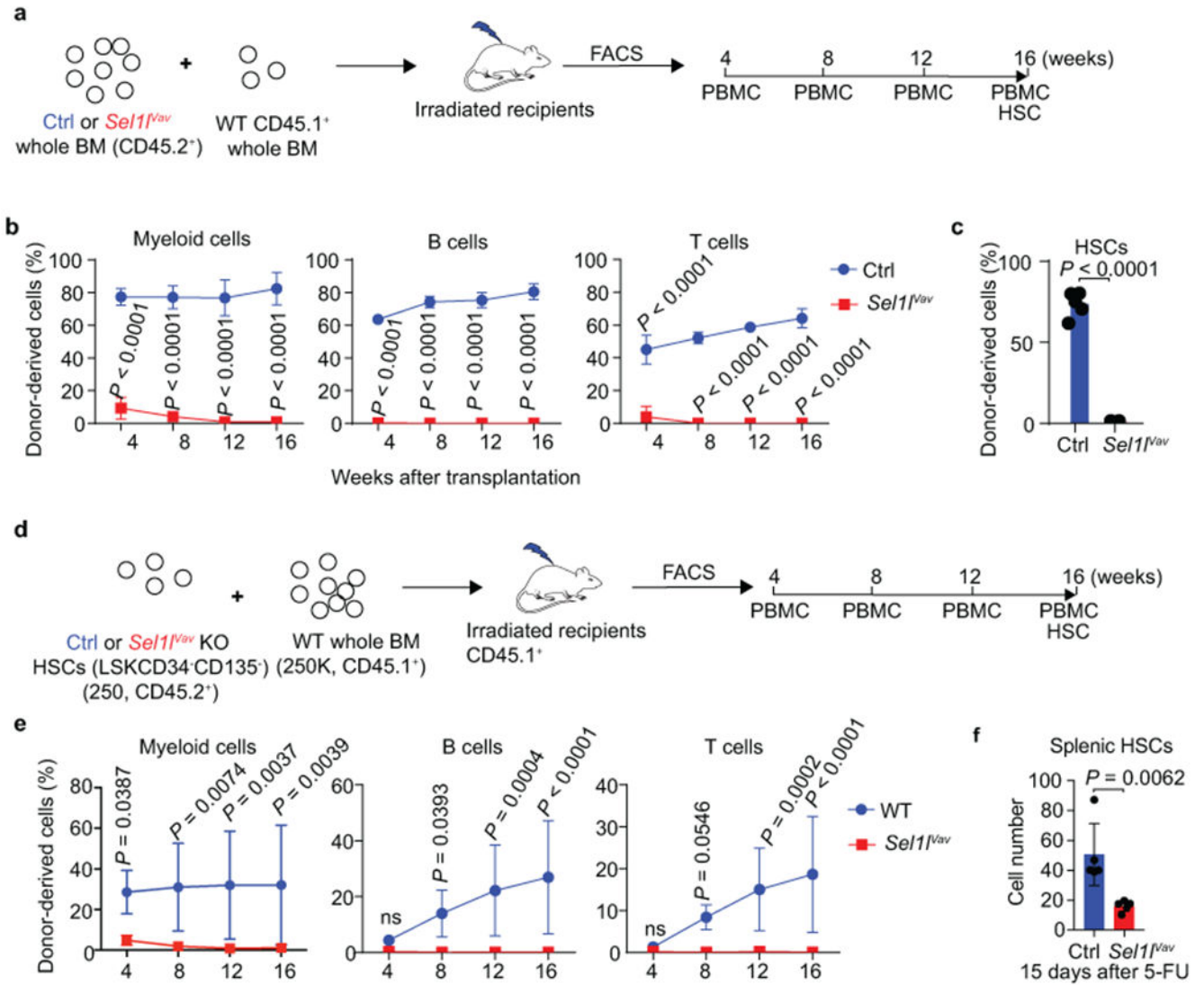
Extended Data Fig. 5. SEL1L is required for HSC regenerative potential under hematological stress condition

a, Schematic depiction of the competitive bone marrow transplantation scheme using whole bone marrow cells. CD45.2[+] donor BM cells isolated from control (Ctrl) or *Sel1l*[Vav] mice were mixed with CD45.1[+] competitor BM cells at 3:1 ratio, transplanted into lethally irradiated CD45.1[+] recipients respectively. Reconstitution levels were monitored for 16 weeks in peripheral blood (PBMC) including myeloid cells, B cells and T cells and HSCs were examined 16 weeks after transplantation. **b, c,** Percentage of donor-derived myeloid cells, B cells and T cells in peripheral blood at indicated time points (**b**) or HSC in the BM at 16 weeks after transplantation (**c**). Week4 in b: $n = 8$; $n = 5$ in all the other time points. $n = 5$ in c. **d**, Schematic depiction of the competitive bone marrow transplantation scheme using LT-HSCs (LSK CD34^{−}Flk2^{−}) as donor. 250 HSCs were mixed with 250,000 CD45.1^{+} BM cells for each recipient mice in this assay. **e**, Percentage of donor-derived myeloid cells, B cells and T cells in peripheral blood at indicated time points using LT-HSC as donor. $n = 7$. **f**, Quantification of HSCs number in the spleen of control (Ctrl) and *Sel1l*[Vav] mice 15 days

after 5-FU treatment. $n = 5$. Results are shown as mean ± s.d. Two-way ANOVA (**b**, **e**, **h**) or two-tailed Student's t-tests (**c**, **f**) were used to assess statistical significance. ns, not significant. Statistical information is provided as source data.
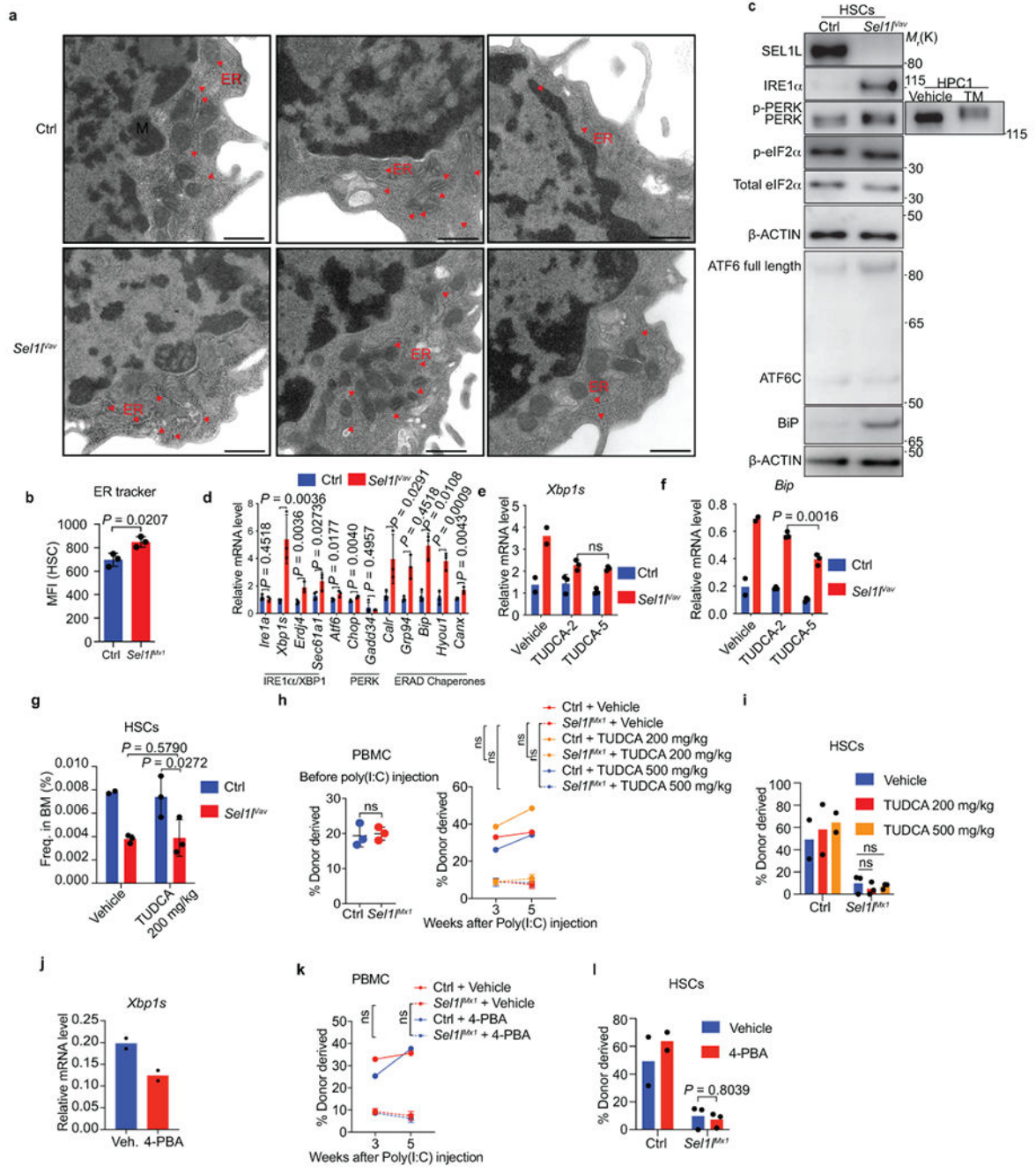
Extended Data Fig. 6. Characterization of ER stress and UPR activation in *Sel1l*-KO HSCs
a, Transmission electron microscopic analysis of the ER and mitochondria (M) in HSCs from Control (Ctrl) or *Sel1l*^Vav^-KO mice. Scale bar, 1 μm. **b**, ER-tracker staining in Ctrl and *Sel1l*^Mx1^ HSCs. $n = 3$. **c**, WB analysis of HSCs from 8-week-old control and *Sel1l*^Vav^-KO

mice. **d**, RT-PCR analysis of UPR and ERAD in 8-week-old control or *Sel1l*^*Vav*^-KO HSCs. Ctrl: $n = 4$; *Sel1l*^*Vav*^: $n = 3$. **e**, **f**, RT-PCR analysis of *Xbp1s* (**e**) and *Bip* (**f**) expression in c-Kit-enriched BM cells from Ctrl and *Sel1l*^*Vav*^-KO mice treated with vehicle or TUDCA (TUDCA-2: 200 mg/kg, TUDCA-5: 500 mg/kg). Vehicle: $n = 2$; TUDCA: $n = 3$. **g**, Frequency of HSCs in vehicle- or TUDCA (200 mg/kg)-treated Ctrl and *Sel1l*^*Vav*^ mice. $n = 2$ for vehicle-treated control group and $n = 3$ for the other 3 groups. **h**, **i**, Percentage of control and *Sel1l*^*Mx1*^ donor-derived PBMC (**h**) and HSCs (**i**) in recipient mice at indicated time after vehicle or TUDCA treatment (daily i.p. injection) starting from the first poly(I:C) injection (4 weeks after donor-reconstitution). HSCs were analyzed at week 5. Ctrl: $n = 2$; *Sel1l*^*Mx1*^: $n = 3$. The Vehicle groups and donor chimerism of $n=3$ randomly sampled mice from control or *Sel1l*^*Mx1*^ donor group before poly(I:C) injection (left panel of **h**) is the same as in **Extended Data Fig.6k**, **l**, **7**, **8**. **j**, RT-PCR analysis of *Xbp1s* expression in LSK cells from 4-PBA treated mice. $n = 2$. **k**, **l**, Percentage of Ctrl and *Sel1l*^*Mx1*^ donor-derived PBMC (**k**) and HSCs (**l**) in recipient mice at indicated time after vehicle or 4-PBA treatment (in drinking water) starting from the first poly(I:C) injection. Ctrl: $n = 2$; *Sel1l*^*Mx1*^: $n = 3$. Results are shown as mean ± s.d. Two-tailed Student's t-tests (**b**, **d**, **j**) or two-way ANOVA with Bonferroni test (**e-i**, **k**, **l**) were used to calculate *P* values. ns, not significant. Statistical information and unprocessed blots are provided as source data.
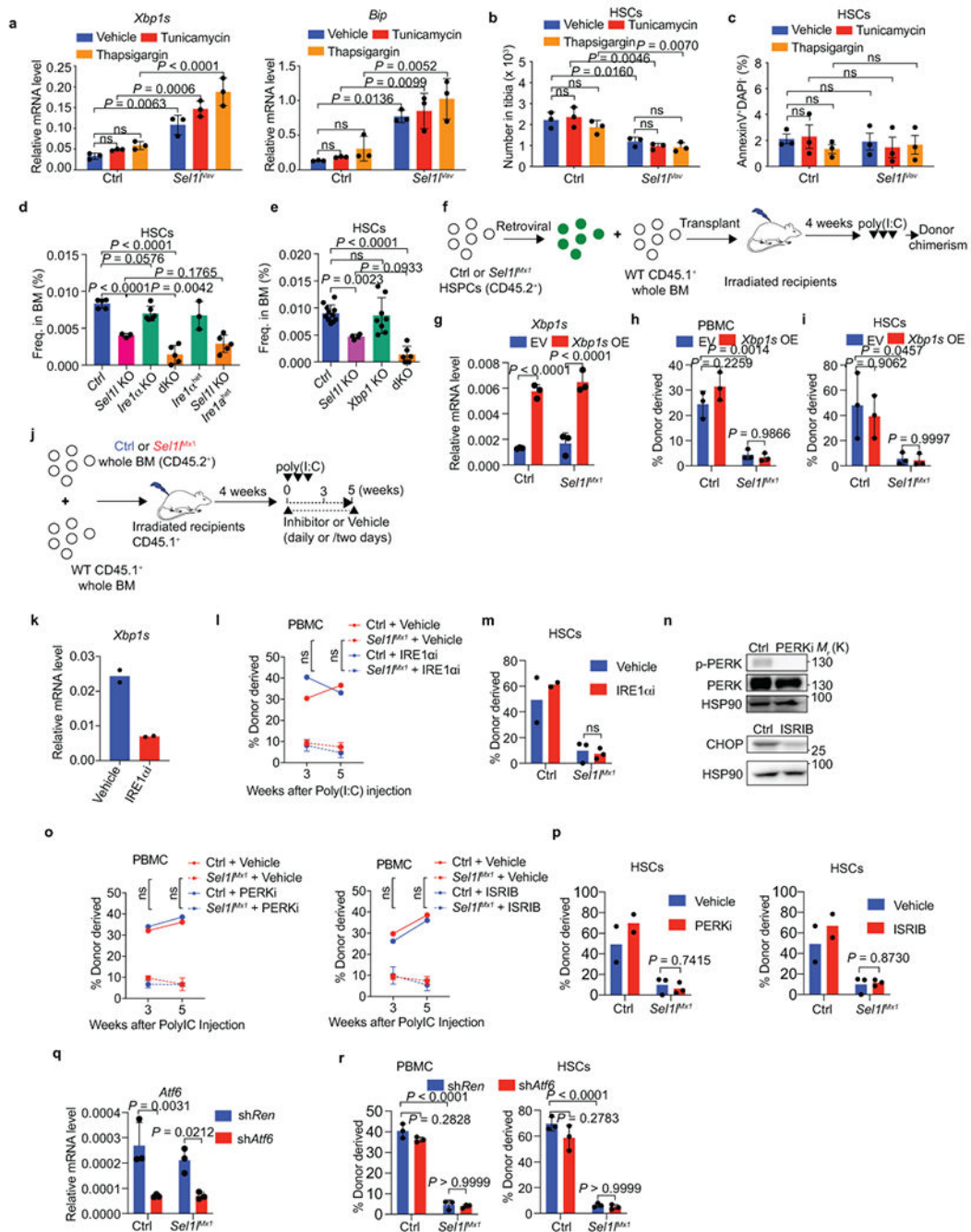
Extended Data Fig. 7. Regulation of HSC identity by SEL1L ERAD is independent of ER stress and UPR

a, Quantification of *Xbp1s* (**left**) and *Bip* (**right**) expression in control (Ctrl) or *Sel1l*[Vav]-KO HSCs treated with tunicamycin (0.1mg/kg) or thapsigargin (0.05 mg/kg) for 4 weeks (i.p. injection, 3 times/week). $n = 3$. **b, c**, Number of HSCs (**b**) and quantification of apoptotic HSCs (**c**) from Ctrl and *Sel1l*[Vav]-KO mice as in **a**. $n = 3$. **d**, Frequency of HSCs in the BM of 8-week-old mice with indicated genotypes. *Sel1l*[f/f]; *Ire1a*[f/f] (Ctrl): $n = 5$; *Sel1l*[Vav] (*Sel1l*-KO): $n = 3$; *Ire1a*[Vav] (*Ire1a*-KO): $n = 6$; *Sel1l; Ire1a* double-knockout (dKO): $n = 5$; *Vav-*

*iCre: Ire1a^het^*, $n = 3$; *Vav-iCre; Sel1l^f/f^; Ire1a^het^*, $n = 5$, data are combined from 2 independent experiments. **e**, Frequency of HSCs in the BM of 8-week-old mice with indicated genotypes. *Sel1l^f/f^; XBP1^f/f^* (Ctrl): $n = 11$, *Sel1l^Vav^* (*Sel1l*-KO): $n = 4$, *Xbp1^Vav^*(*Xbp1*-KO): $n = 8$, *Sel1l; Xbp1* double-knockout (dKO): $n = 6$, data are combined from 3 independent experiments. **f**, Schematic of BMT assay using retroviral transduced HSPCs. **g**, Quantification of *Xbp1*s expression in Ctrl and *Sel1l^Mx1^*-KO HSPCs transduced by empty vector (EV) or *Xbp1s*. $n = 3$ independent samples. **h, i**, Percentage of Ctrl and *Sel1l^Mx1^*-KO donor-derived PBMC (**h**) and HSCs (**i**) transduced with indicated construct in recipient mice. $n = 3$. **j**. Schematic of treatment strategy for competitive BMT assay. **k**, Quantification of *Xbp1s* expression in vehicle or IRE1α inhibitor MKC8866 (IRE1αi) treated HSCs. HSCs were sorted from Ctrl + Vehicle or Ctrl + IRE1αi group at the end of the rescue experiments. $n = 2$. **l, m**, Percentage of Ctrl and *Sel1l^Mx1^* donor-derived PBMC (**l**) and HSCs in the BM (**m**) of recipient mice at the indicated time points. HSCs were analyzed at week 5. Ctrl: $n = 2$; *Sel1l^Mx1^*: $n = 3$. **n**, WB analysis of p-PERK and CHOP in WBM cells from mice treated with PERK inhibitor GSK2656157 (PERKi) or eIF2α inhibitor ISRIB respectively as in **j**. **o, p**, Percentage of Ctrl and *Sel1l^Mx1^* donor-derived PBMC (**o**) and HSCs (**p**) in recipient mice treated with vehicle, PERKi or ISRIB at the indicated time points. HSCs were analyzed at week 5. Ctrl: $n = 2$; *Sel1l^Mx1^*: $n = 3$. **q**, Quantification of Atf6 expression in Ctrl and *Sel1l^Mx1^* HSPCs transduced with control shRNA (shRen) or shRNA targeting Atf6 (shAtf6). $n = 3$ independent samples. **r**, Percentage of Ctrl and *Sel1l^Mx1^* donor-derived PBMC (**left**) and HSCs (**right**) in recipient mice transduced with indicated construct. $n = 3$. The same vehicle group was used in **l, m, o, p**. Two-way ANOVA (**a-c, g-i**, **l, m, o-r**), one-way ANOVA (**d, e**) or two-tailed Student's t-tests (**k**) were used to calculate *P* values. Results are shown as mean ± s.d or mean ± s.e.m (**c**). Statistical information and unprocessed blots are provided as source data.
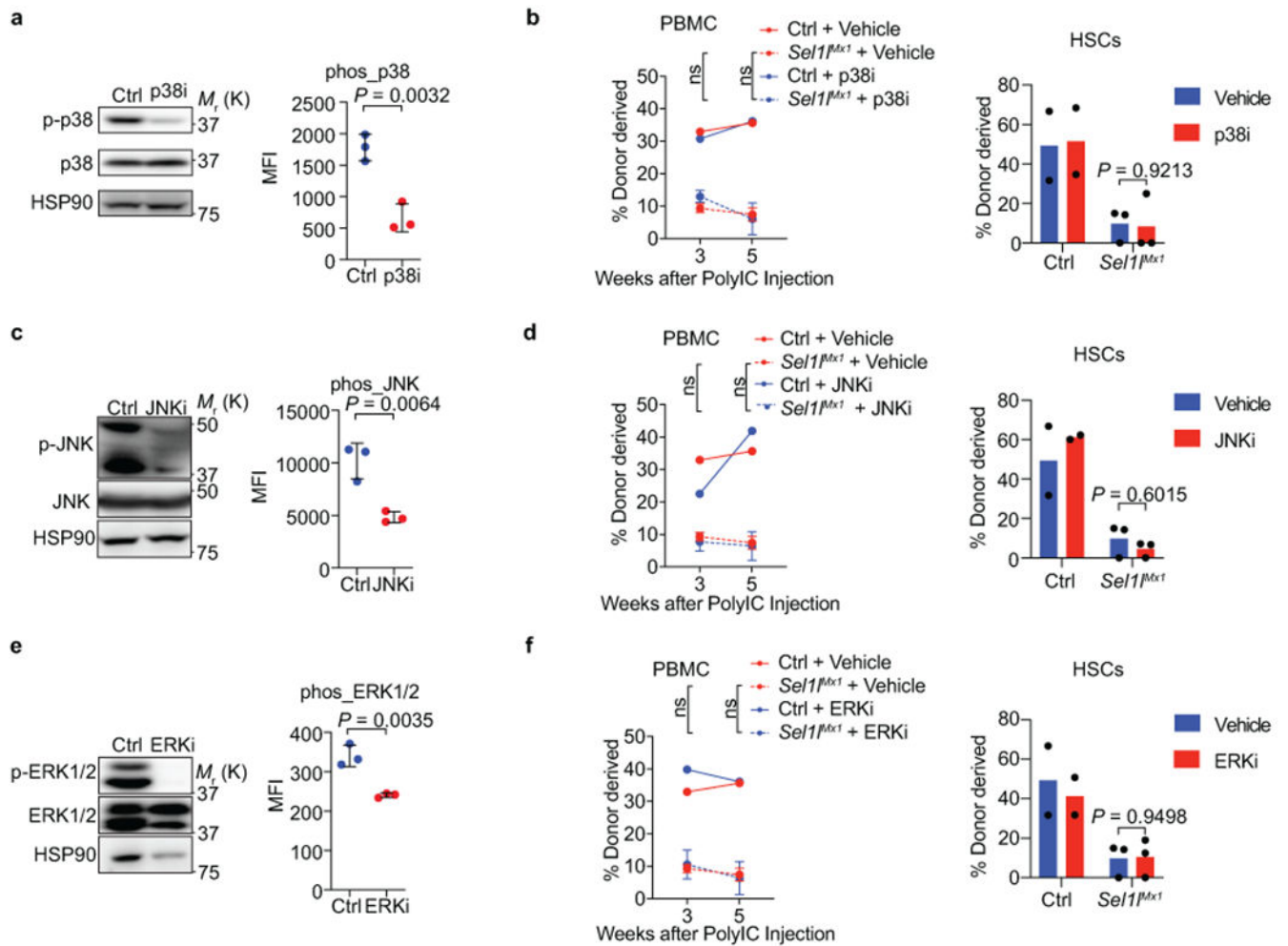
Extended Data Fig. 8. Regulation of HSC identity by SEL1L ERAD is independent of MAPK signaling

a, Analysis of p-p38 levels in whole bone marrow (WBM) by western blot (**left**) or in HSCs by flow cytometry from mice treated with vehicle or p38 inhibitor SB202190 (p38i). For flow analysis, $n = 3$ (3 of the 5 vehicle or p38i treated mice were randomly picked and donor-competitor HSCs were not distinguished). **b**, Percentage of control (Ctrl) and $Sel1l^{Mx1}$ donor-derived PBMC (**left**) and HSCs in the BM (**right**) of recipient mice treated with vehicle or p38i at the indicated time points. HSCs were analyzed at week 5. Ctrl: $n = 2$; $Sel1l^{Mx1}$: $n = 3$. **c**, Analysis of p-JNK levels in WBM by western blot (**left**) or in HSCs by flow cytometry from mice treated by vehicle or JNK inhibitor SP600125 (JNKi). $n = 3$. **d**, Percentage of control (Ctrl) and $Sel1l^{Mx1}$ donor-derived PBMC (**left**) and HSCs in the BM (**right**) of recipient mice treated with vehicle or JNKi at the indicated time points. HSCs were analyzed at week 5. Ctrl: $n = 2$; $Sel1l^{Mx1}$: $n = 3$. **e**, Analysis of p-ERK1/2 levels in WBM by western blot (**left**) or in HSCs by flow cytometry from mice treated with vehicle or ERK1/2 inhibitor SCH772984 (ERKi). $n = 3$. **f**, Percentage of control (Ctrl) and $Sel1l^{Mx1}$ donor-derived PBMC (**left**) and HSCs in the BM (**right**) of recipient mice treated with vehicle or ERKi at the indicated time points. HSCs were analyzed at week 5. Ctrl: $n = 2$;

$Sel1l^{Mx1}$: $n = 3$. The same vehicle group was used in **b**, **d** and **f**. Two-way ANOVA (**b**, **d** and **f**), or two-tailed Student's t-tests (**a**, **c** and **e**) were used to calculate P values. Results are shown as mean ± s.d. Statistical information and unprocessed blots are provided as source data.
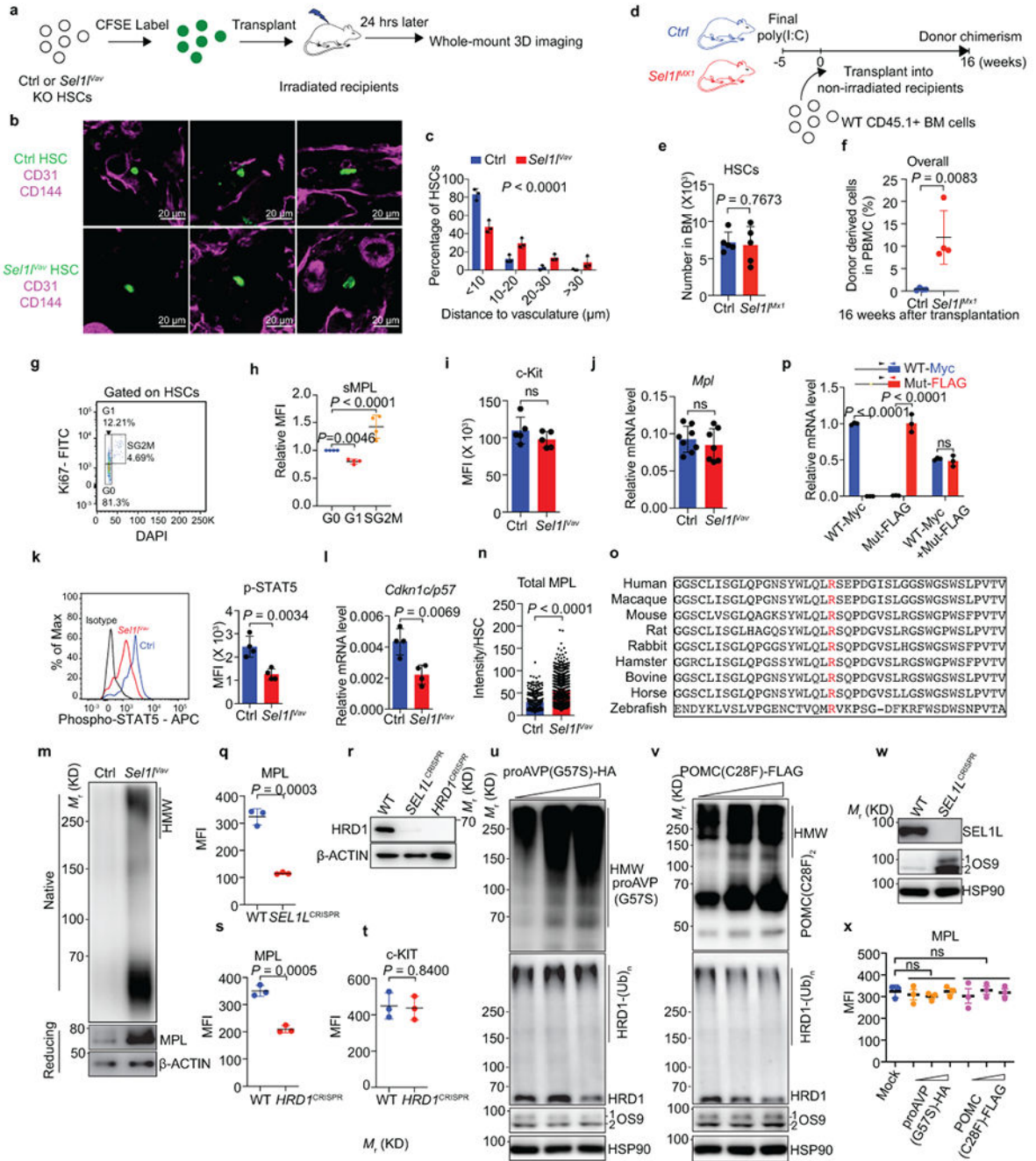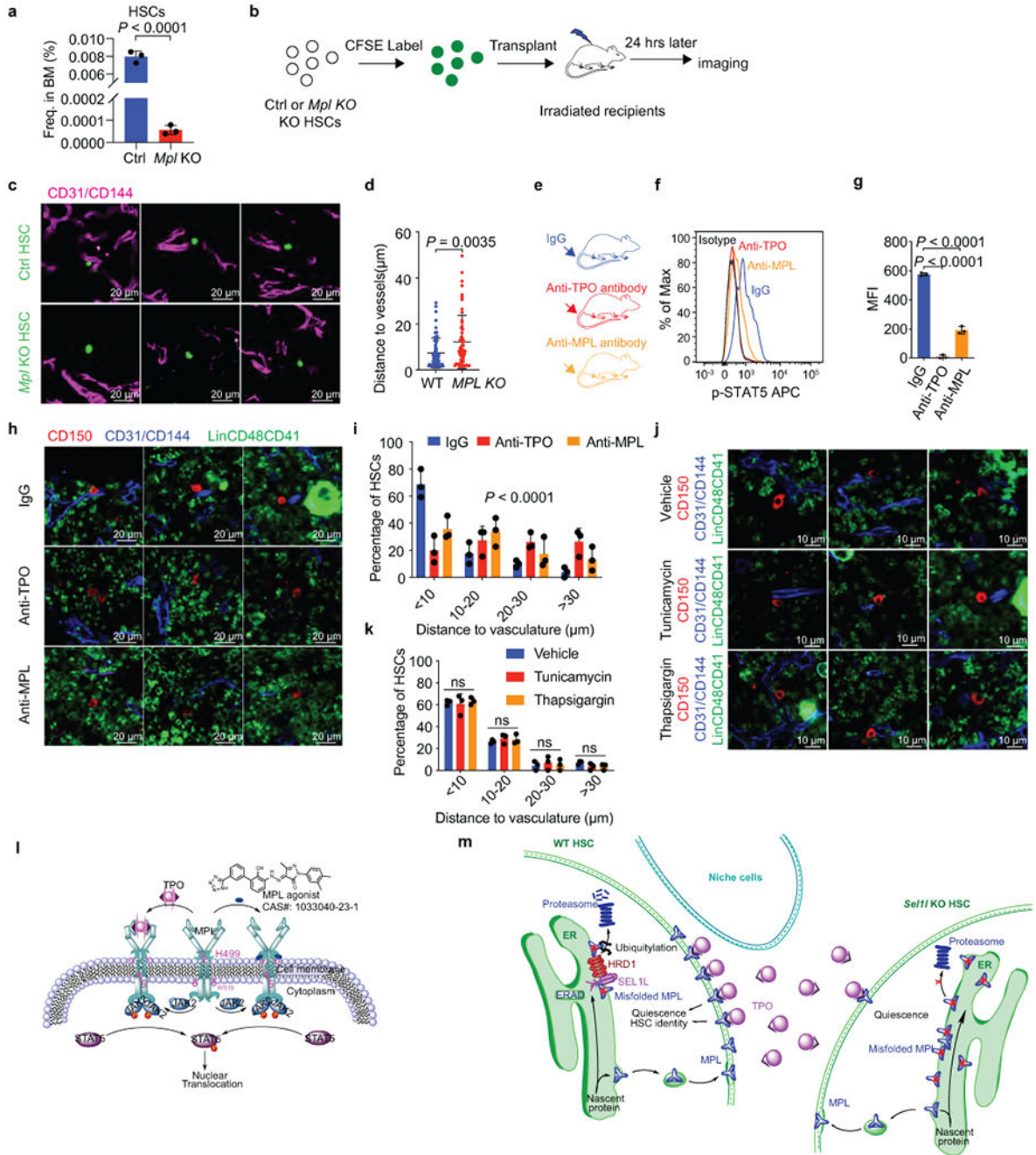

Extended Data Fig. 9. SEL1L regulates MPL maturation

a, Schematic of HSC (LSK CD150⁺CD48⁻)-vasculature distance measurement in the BM.

b, **c**, Representative 2D images (**b**) and quantification (**c**) of the distances between CFSE-

labelled HSCs (green) and vascular structure (CD31^{+} and/or CD144^{+}, magenta). 177 control (Ctrl) and 147 $Sel1l^{Vav}$-KO HSCs were analyzed over n=3 independent experiments. Scale bar, 20 μm. **d**, Schematic for non-conditioned transplantation of donor cells into Ctrl or $Sel1l^{Mx1}$-KO congenic mice. **e**, The HSCs numbers in Ctrl and $Sel1l^{Mx1}$-KO mice 5 weeks after poly (I:C) injection. $n = 5$. **f**, Percentage of donor-derived (CD45.1^{+}) cells in the PBMC of non-irradiated Ctrl or $Sel1l^{Mx1}$-KO recipient mice 16 weeks after transplantation. $n = 4$. **g**, **h**, Flow analysis of surface MPL expression in HSCs at different cell cycle states. Representative flow cytometry plots (**g**) and quantification (**h**) are shown. $n = 4$. **i**, Quantification of surface c-Kit expression from 8-week-old Ctrl and $Sel1l^{Vav}$-ko HSCs. $n = 5$. **j**, RT-PCR analysis of Mpl mRNA in 8-week-old Ctrl or $Sel1l^{Vav}$-KO HSCs. Data are presented relative to $Actb$. Ctrl: $n = 8$; $Sel1l^{Vav}$: $n = 7$. **k**, Representative histogram and quantification of phospho-STAT5 (Tyr694) level from 30-week-old Ctrl or $Sel1l^{Vav}$-KO HSCs. $n = 4$. **l**, Quantification of $p57$ mRNA by qPCR in 8-week-old Ctrl or $Sel1l^{Vav}$-KO HSCs. $n = 4$. **m**, WB analysis of total MPL in HSCs from 8-week-old Ctrl and $Sel1l^{Vav}$-KO mice under native or denature conditions. **n**, Quantification of total MPL signal in Ctrl and $Sel1l^{Vav}$-KO HSCs from immunostaining experiment in Fig. 4f. Ctrl HSCs: $n = 100$; $Sel1l^{Vav}$ HSCs: $n = 250$. **o**, Sequence alignment of MPL from indicated species with R257 (Human) highlighted in red. **p**, 293T cells were transfected with Myc-tagged wildtype MPL (WT-Myc), FLAG-tagged mutant MPL (Mut-FLAG) or 1:1-mixed WT and Mut MPL (WT-Myc + Mut-FLAG) for 48h. The expression of WT or Mutant MPL was quantified by qPCR primers specific to Myc or FLAG tag. $n = 3$ independent samples. **q**, WT or $SEL1L^{CRISPR}$-KO 293T cells were transfected with HA-tagged MPL and surface MPL expression was determined by flow cytometry 48h later. $n = 3$. **r**, WB analysis of HRD1 expression in WT, $SEL1L^{CRISPR}$-KO or $HRD1^{CRISPR}$-KO 293T cells. **s**, **t**, WT or $HRD1^{CRISPR}$-KO 293T cells were transfected with HA-tagged MPL and surface MPL or C-KIT expression were determined by flow cytometry 48h after transfection. $n = 3$. **u-x**, Expression of aggregation-prone mutant proAVP (G57S) (**u**) or POMC (C28F) (**v**) forms aggregates in WT 293T cells, but is not sufficient to inhibit ERAD activity (**u**, **v**, **w**) and thus does not reduce surface MPL expression (**x**). HRD1 autoubiquitination (**u**, **v**) and OS9 (OS9–1 and OS9–2) accumulation (**u**, **v**, **w**) were used as validated indicators for ERAD activity. The experiments for **q** and **u-x** are performed together, the MPL level in WT (**r**) and Mock (**x**) was from the same experiment. n=3. Results are shown as mean ± s.d. Two-tailed Student's t-test (**e**, **f**, **h-l**, **n**, **p**, **q**, **s**, **t**, **x**), or two-sample Kolmogorov–Smirnov test (**c**) were used to assess statistical significance. ns, not significant. Statistical information and unprocessed blots are provided as source data.

Extended Data Fig. 10: MPL-TPO is important for HSC-niche interaction

a, Frequency of HSCs in 20-week-old control (Ctrl) and *Mpl*-KO mice. *n* = 3. **b**, Schematic of HSC (LSK CD150$^+$CD48$^−$)-vasculature distance measurement in the BM. Donor HSCs were analyzed by whole-mount confocal microscope in femurs and tibiae. **c, d**, Representative 2D images (**c**) and quantification (**d**) of the distances between CFSE-labelled HSCs (green) and vascular structure (CD31$^+$ and/or CD144$^+$, magenta). A total of n=71 Ctrl and n=57 *Mpl*-KO HSCs were analyzed over 3 independent experiments. Scale bar, 20 μm. **e**, Mice were treated by indicated antibodies daily for 7 days before examining the HSC-

vasculature distance in the BM. **f**, **g**, Both MPL and TPO antibodies blocked TPO-induced phospho-STAT5 in HSCs in vitro. $n = 3$ independent samples. **h**, **i**, Representative 2D images (**h**) and quantification (**i**) of the distances between indicated HSCs (CD150$^+$Lin$^-$CD48$^-$CD41$^-$, Red) and the closest vascular structure (CD31$^+$ and/or CD144$^+$, Blue). HSCs from mice treated with IgG control (combined, total of 71 HSCs), anti-TPO antibody (total of 83 HSCs) or anti-MPL antibody (total of 73 HSCs) were analyzed in $n = 3$ independent experiments for all groups. Scale bar, 20 μm. **j**, **k**, Representative 2D images (**j**) and quantification (**k**) of the distance between indicated HSCs (Red) and the closest vascular structure (Blue). HSCs from mice treated with vehicle (total = 123), tunicamycin (total = 101) or thapsigargin (total = 98) were analyzed. $n = 3$ independent samples. Scale bar, 10 μm. **l**, Diagram showing the structure of MPL agonist and its binding to the juxtamembrane end of MPL. **m**, Schema depicting the regulation of HSC identity by SEL1L-HRD1 ERAD. Results are shown as mean ± s.d. Two-tailed Student's t-test (**a**, **d**, **g**), or two-sample Kolmogorov–Smirnov test (**i**, **k**) were used to assess statistical significance. ns, not significant. Statistical information and unprocessed blots are provided as source data.

Supplementary Material

Refer to Web version on PubMed Central for supplementary material.

Acknowledgements.

REFERENCES:

1. Garcia-Prat L, Sousa-Victor P & Munoz-Canoves P Proteostatic and Metabolic Control of Stemness. Cell Stem Cell 20, 593–608 (2017). [PubMed: 28475885]

2. Vilchez D, Saez I & Dillin A The role of protein clearance mechanisms in organismal ageing and age-related diseases. Nat Commun 5, 5659 (2014). [PubMed: 25482515]

3. Bakker ST & Passegue E Resilient and resourceful: genome maintenance strategies in hematopoietic stem cells. Exp Hematol 41, 915–923 (2013). [PubMed: 24067363]

4. Brodsky JL Cleaning up: ER-associated degradation to the rescue. Cell 151, 1163–1167 (2012). [PubMed: 23217703]

5. Morrison SJ & Scadden DT The bone marrow niche for haematopoietic stem cells. Nature 505, 327–334 (2014). [PubMed: 24429631]

6. Yoshida H et al. The cis-Regulatory Atlas of the Mouse Immune System. Cell 176, 897–912 e820 (2019). [PubMed: 30686579]

7. Lara-Astiaso D et al. Chromatin state dynamics during blood formation. Science 345, 943–949 (2014). [PubMed: 25103404]

8. Schinzel RT et al. The Hyaluronidase, TMEM2, Promotes ER Homeostasis and Longevity Independent of the UPRER. Cell 179, 1306–1318.e1318 (2019). [PubMed: 31761535]

9. Ehninger A et al. Loss of SPARC protects hematopoietic stem cells from chemotherapy toxicity by accelerating their return to quiescence. Blood 123, 4054–4063 (2014). [PubMed: 24833352]

10. Sigurdsson V et al. Bile Acids Protect Expanding Hematopoietic Stem Cells from Unfolded Protein Stress in Fetal Liver. Cell Stem Cell 18, 522–532 (2016). [PubMed: 26831518]

11. van Galen P et al. The unfolded protein response governs integrity of the haematopoietic stem-cell pool during stress. Nature 510, 268–272 (2014). [PubMed: 24776803]

12. Miharada K, Sigurdsson V & Karlsson S Dppa5 Improves Hematopoietic Stem Cell Activity by Reducing Endoplasmic Reticulum Stress. Cell Reports 7, 1381–1392 (2014). [PubMed: 24882002]

13. Karagoz GE, Acosta-Alvear D & Walter P The Unfolded Protein Response: Detecting and Responding to Fluctuations in the Protein-Folding Capacity of the Endoplasmic Reticulum. Cold Spring Harb Perspect Biol (2019).

14. Sun S et al. IRE1alpha is an endogenous substrate of endoplasmic-reticulum-associated degradation. Nat Cell Biol 17, 1546–1555 (2015). [PubMed: 26551274]

15. Qi L, Tsai B & Arvan P New Insights into the Physiological Role of Endoplasmic Reticulum-Associated Degradation. Trends in Cell Biology 27, 430–440 (2017). [PubMed: 28131647]

16. Cortez L & Sim V The therapeutic potential of chemical chaperones in protein folding diseases. Prion 8 (2014).

17. Zhao N et al. Pharmacological targeting of MYC-regulated IRE1/XBP1 pathway suppresses MYC-driven breast cancer. J Clin Invest 128, 1283–1299 (2018). [PubMed: 29480818]

18. Sidrauski C et al. Pharmacological brake-release of mRNA translation enhances cognitive memory. eLife 2, e00498 (2013). [PubMed: 23741617]

19. Pinho S & Frenette PS Haematopoietic stem cell activity and interactions with the niche. Nat Rev Mol Cell Biol 20, 303–320 (2019). [PubMed: 30745579]

20. Walter P & Ron D The unfolded protein response: from stress pathway to homeostatic regulation. Science 334, 1081–1086 (2011). [PubMed: 22116877]

21. Acar M et al. Deep imaging of bone marrow shows non-dividing stem cells are mainly perisinusoidal. Nature 526, 126–130 (2015). [PubMed: 26416744]

22. Kunisaki Y et al. Arteriolar niches maintain haematopoietic stem cell quiescence. Nature 502, 637–643 (2013). [PubMed: 24107994]

23. Ballmaier M & Germeshausen M Advances in the understanding of congenital amegakaryocytic thrombocytopenia. British Journal of Haematology 146, 3–16 (2009). [PubMed: 19388932]

24. Varghese LN, Defour JP, Pecquet C & Constantinescu SN The Thrombopoietin Receptor: Structural Basis of Traffic and Activation by Ligand, Mutations, Agonists, and Mutated Calreticulin. Front Endocrinol (Lausanne) 8, 59 (2017). [PubMed: 28408900]

25. Fox NE, Lim J, Chen R & Geddis AE F104S c-Mpl responds to a transmembrane domain-binding thrombopoietin receptor agonist: proof of concept that selected receptor mutations in congenital amegakaryocytic thrombocytopenia can be stimulated with alternative thrombopoietic agents. Exp Hematol 38, 384–391 (2010). [PubMed: 20188141]

26. Hidalgo San Jose L et al. Modest Declines in Proteome Quality Impair Hematopoietic Stem Cell Self-Renewal. Cell Reports 30, 69–80.e66 (2020). [PubMed: 31914399]

27. Signer RA, Magee JA, Salic A & Morrison SJ Haematopoietic stem cells require a highly regulated protein synthesis rate. Nature 509, 49–54 (2014). [PubMed: 24670665]

28. Iwawaki T, Akai R, Yamanaka S & Kohno K Function of IRE1 alpha in the placenta is essential for placental development and embryonic viability. Proc Natl Acad Sci U S A 106, 16657–16662 (2009). [PubMed: 19805353]

29. Lee AH, Scapa EF, Cohen DE & Glimcher LH Regulation of hepatic lipogenesis by the transcription factor XBP1. Science 320, 1492–1496 (2008). [PubMed: 18556558]

30. Sun S et al. Sel1L is indispensable for mammalian endoplasmic reticulum-associated degradation, endoplasmic reticulum homeostasis, and survival. Proc Natl Acad Sci U S A 111, E582–591 (2014). [PubMed: 24453213]

31. Murone M, Carpenter DA & de Sauvage FJ Hematopoietic Deficiencies in c-mpl and TPO Knockout Mice. STEM CELLS 16, 1–6 (1998).

32. Miller CL, Dykstra B & Eaves CJ Characterization of Mouse Hematopoietic Stem and Progenitor Cells. Current Protocols in Immunology 80, 22B.22.21–22B.22.31 (2008).

33. Kankaanpaa P et al. BioImageXD: an open, general-purpose and high-throughput image-processing platform. Nat Methods 9, 683–689 (2012). [PubMed: 22743773]

34. Kawamoto T Use of a new adhesive film for the preparation of multi-purpose fresh-frozen sections from hard tissues, whole-animals, insects and plants. Arch Histol Cytol 66, 123–143 (2003). [PubMed: 12846553]

35. Kumar S & Filippi MD An Alternative Approach for Sample Preparation with Low Cell Number for TEM Analysis. J Vis Exp (2016).

36. Fellmann C et al. An Optimized microRNA Backbone for Effective Single-Copy RNAi. Cell Reports 5, 1704–1713 (2013). [PubMed: 24332856]

37. Sun S et al. IRE1alpha is an endogenous substrate of endoplasmic-reticulum-associated degradation. Nat Cell Biol 17, 1546–1555 (2015). [PubMed: 26551274]

38. Nakada D, Saunders TL & Morrison SJ Lkb1 regulates cell cycle and energy metabolism in haematopoietic stem cells. Nature 468, 653 (2010). [PubMed: 21124450]

39. Betts S, Speed M & King J Detection of early aggregation intermediates by native gel electrophoresis and native Western blotting, in Methods in Enzymology, Vol. 309 333–350 (Academic Press, 1999). [PubMed: 10507034]
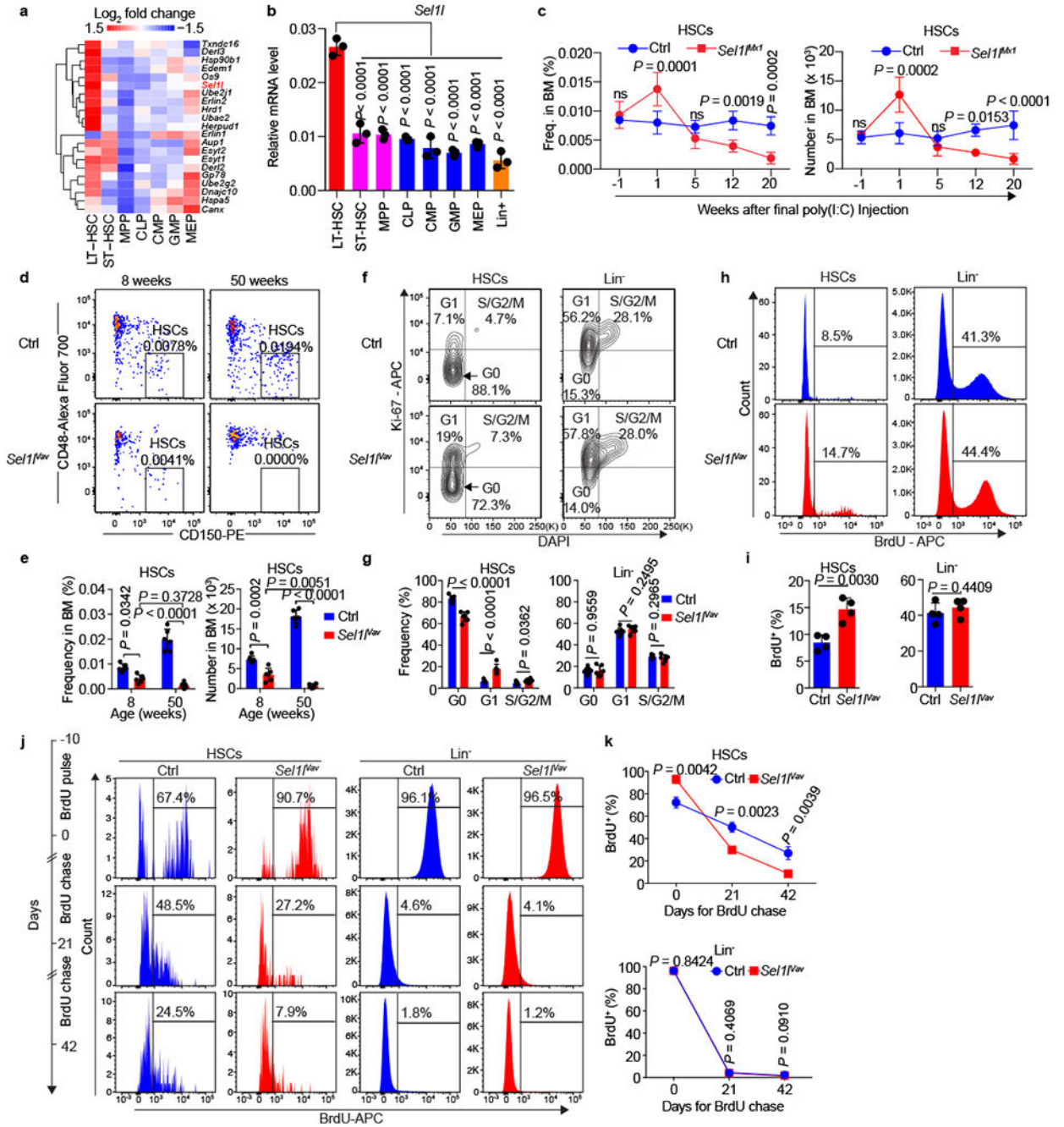
**Figure 1 |. SEL1L is highly expressed and required for the steady-state HSC**

a, Heatmap showing the expression profile of ERAD-related genes in mouse HSCs and progenitor cells. LT-HSC: long-term HSC (LSK CD34$^-$Flk2$^-$); ST-HSC: short-term HSC (LSK CD34$^+$Flk2$^-$); MPP: multipotent progenitors (LSK CD34$^+$Flk2$^+$); CLP: common lymphoid progenitors (Lin$^-$Sca-1^{low}c-Kit^{low}Flk2$^+$IL7Rα$^+$); CMP: common myeloid progenitors (LS-K CD34$^+$FcγR$^-$); GMP: granulocyte/macrophage progenitors (LS-K CD34$^+$FcγR$^+$); MEP: megakaryocytic/erythroid progenitors (LS-K CD34$^-$FcγR$^-$). Data are extracted from GSE60101. **b**, Quantitative RT-PCR analysis of *Sel1l* expression in mouse

HSCs and progenitors. Data are presented relative to *Gapdh*. $n = 3$. **c**, Frequency and absolute number of HSCs (LSK CD150$^+$CD48$^−$) in the bone marrow (BM) of control (Ctrl, *Sel1l$^{flox/flox}$*) and *Sel1l^{Mx1}* KO (*Sel1l$^{flox/flox}$*; *Mx1-Cre*) mice at different time points after final poly(I:C) injection, −1 indicates 1 week before poly (I:C) injection. Ctrl: $n = 4$ for time points −1 and 1, $n = 5$ for the other time points; *Sel1l^{Mx1}*: $n = 4$. **d**, **e**, Representative pseudo color dot plots (**d**) and quantification (**e**) of HSCs frequency and number in 8-week-old and 50-week-old control (Ctrl, *Sel1l$^{flox/flox}$*) or *Sel1l^{Vav}* KO (*Sel1l$^{flox/flox}$*; *Vav-icre*) mice. $n = 6$. **f**, **g**, Cell cycle analysis of HSCs and Lin$^−$ cells in 8-week-old *Ctrl* and *Sel1l^{Vav}* KO mice using Ki67 and DAPI. Representative flow cytometry plots (**f**) and quantification (**g**) are shown. *Ctrl*: $n = 7$; *Sel1l^{Vav}*: $n = 6$. **h**, **i**, BrdU incorporation in HSCs and Lin$^−$ cells from 8-week-old *Ctrl* or *Sel1l^{Vav}* KO mice. Representative flow cytometry plots (**h**) and quantification (**i**) of the BrdU$^+$ HSCs or Lin$^−$ cells are shown. $n = 4$. **j**, **k**, Schematic diagram of the BrdU label retention assay, representative flow cytometry plots (**j**) and quantification (**k**) of BrdU$^+$ HSCs and Lin$^−$ cells from *Ctrl* or *Sel1l^{Vav}* KO BM at indicated time points. Ctrl-Day42: $n = 4$; all the others: $n = 3$. n means independent mice. One-way ANOVA (**b**), two-tailed Student's t-tests (**g**, **i**) or two-way ANOVA (**c**, **e**, **k**) was used to calculate P values. Results are shown as mean ± s.d. ns, not significant. Statistical information is provided as source data.
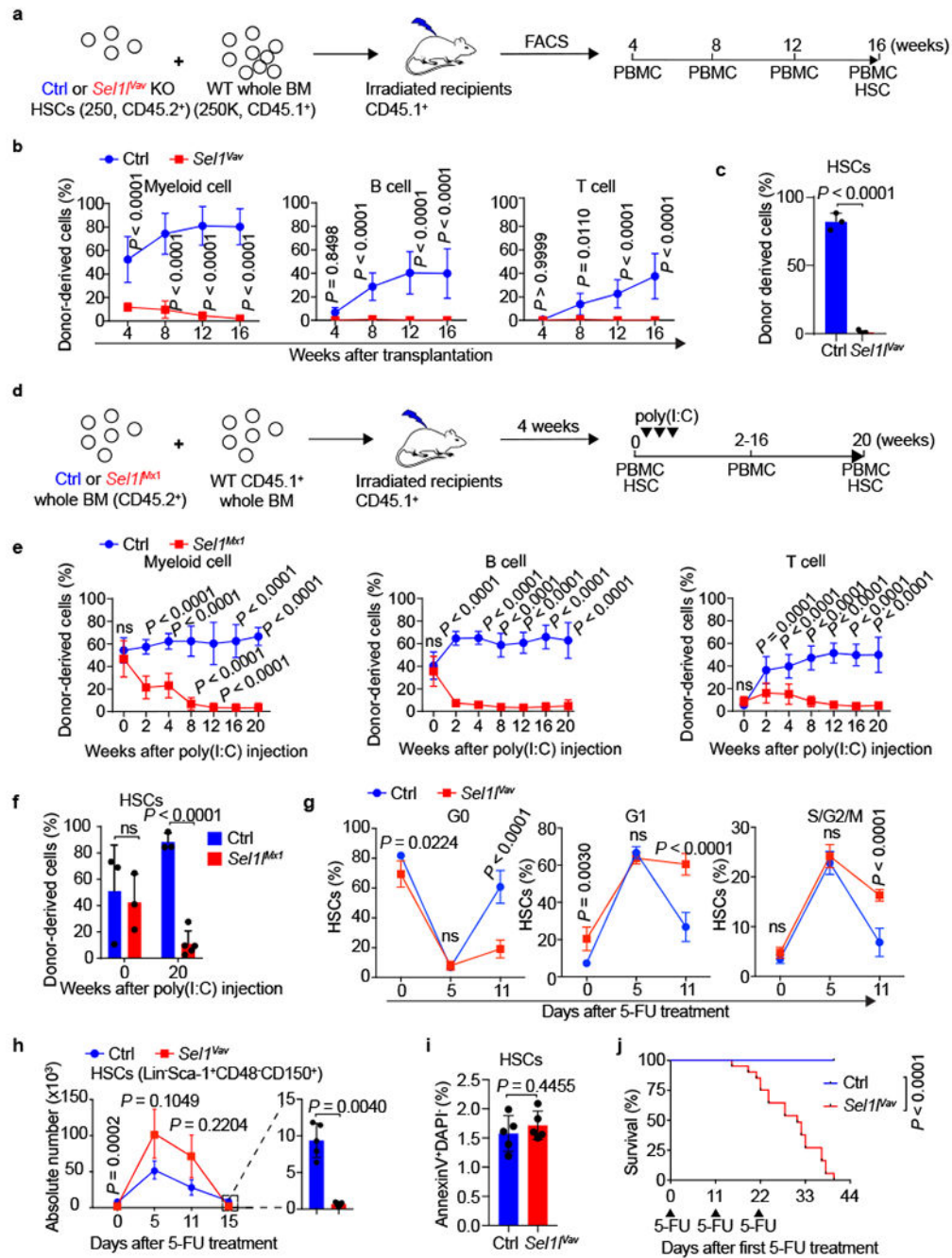
Figure 2 |. SEL1L is required for HSC regenerative potential under hematopoietic stress

a, Schematic depiction of the competitive bone marrow transplantation (BMT) experiment using sorted HSCs (LSK CD150$^+$CD48$^-$) from control (*Ctrl*) or *Sel1l*^{Vav} KO mice as donor. **b**, Percentage of *Ctrl* or *Sel1l*^{Vav} KO donor-derived cells in the peripheral blood of recipient mice at indicated time points. $n = 8$. **c**, Percentage of *Ctrl* or *Sel1l*^{Vav} KO donor derived HSCs in the BM of recipient mice 16 weeks after transplantation. $n = 3$. **d**, Schematic depiction of the competitive BMT experiment using BM cells from *Ctrl* or *Sel1l*^{Mx1} mice. Poly(I:C) was injected 4 weeks after transplantation. **e**, Percentage of *Ctrl* or *Sel1l*^{Mx1}

donor-derived cells in the peripheral blood of recipient mice at indicated time points. *Ctrl*: week 0 and 20, $n = 3$; week 2–16, $n = 6$. *Sel1l^{Mx1}*: week 0, $n = 3$; week 2–16, $n = 8$; week 20: $n = 5$. **f**, Percentage of *Ctrl* or *Sel1l^{Mx1}* donor-derived HSCs in the BM of recipient mice at indicated time points. Week 0, $n = 3$; Week 20, *Ctrl*: $n = 3$; *Sel1l^{Mx1}*: $n = 5$. **g, h**, Percentage of *Ctrl* or *Sel1l^{Vav}* KO HSCs (Lin⁻Sca-1⁺CD48⁻CD150⁺) in G0, G1 and S/G2/M phases of cell cycle and HSCs number at indicated time points after single 5-FU treatment. Day 0: $n = 4$; Day 5: $n = 5$; Day 11: *Ctrl*, $n = 3$, *Sel1l^{Vav}* KO, $n = 4$; Day 15: $n = 5$. **i**, Percentage of apoptotic HSCs in the BM of *Ctrl* or *Sel1l^{Vav}* KO mice 15 days after single 5-FU treatment. $n = 5$. **j**, Kaplan-Meier survival plot of *Ctrl* or *Sel1l^{Vav}* KO mice treated with 3 doses of 5-FU. *Ctrl*: $n = 18$; *Sel1l^{Vav}* KO: $n = 20$. Arrows indicate 5-FU injections. n means independent mice. Two-way ANOVA (**b**, **e**-**g**, **h**) with Bonferroni test, two-tailed Student's t-tests (**c**, **i**) or log-rank test (**j**) was used to calculate P values. Results are shown as mean ± s.d. ns, not significant. Statistical information is provided as source data.
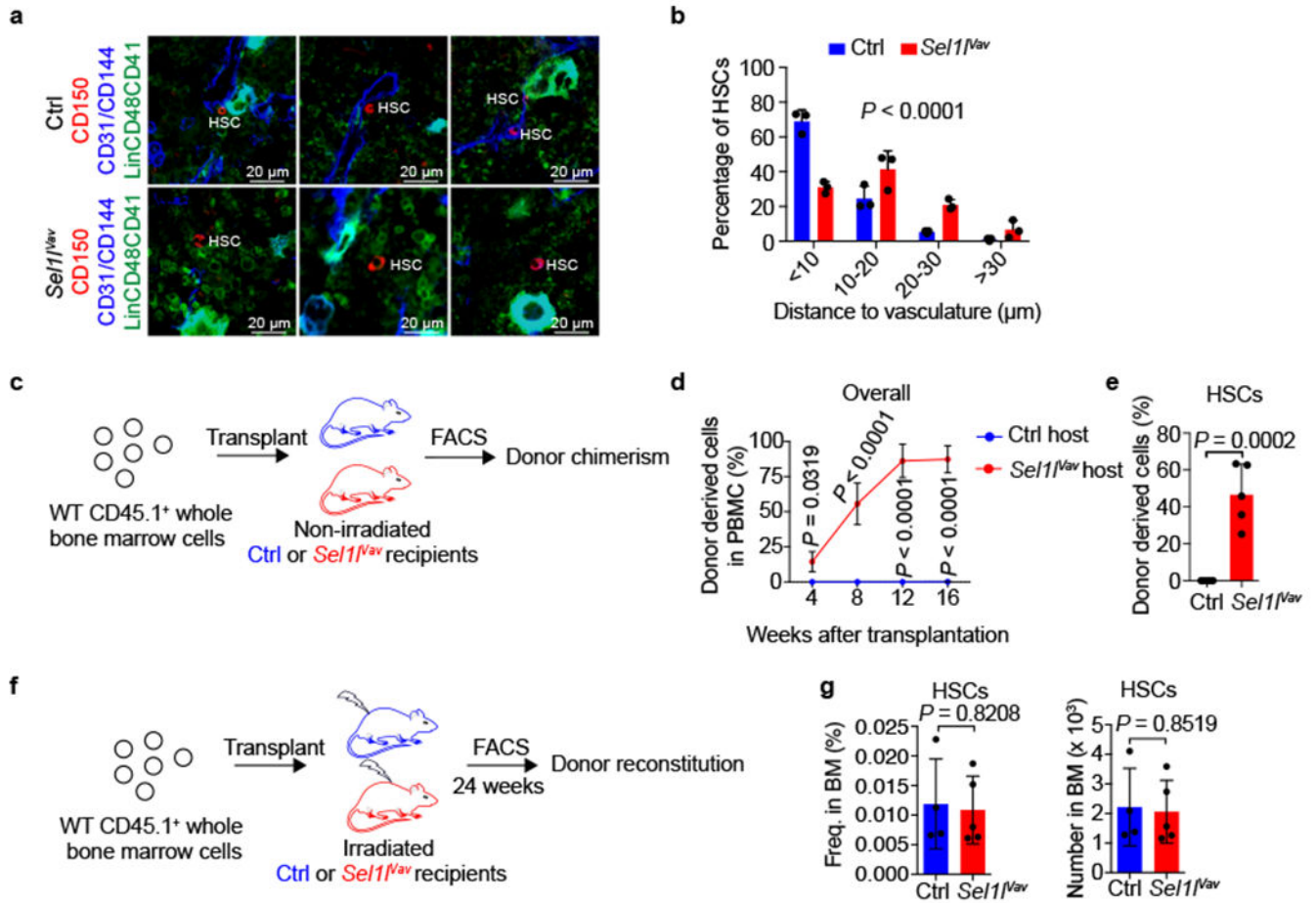
Figure 3 |. SEL1L regulates HSC-niche interaction.
a, **b**, Representative 2D images (**a**) and quantification (**b**) of the distances between HSCs (CD150$^+$Lin$^-$CD48$^-$CD41$^-$, Red) and the closest vascular structure (CD31$^+$ and/or CD144$^+$, Blue). A total of 150 control (*Ctrl*) or 126 *Sel1l*^{Vav} KO HSCs were analyzed in *n*=3 independent experiments. Scale bar, 20 μm. **c**, Experimental schematic for non-conditioned transplantation of donor cells into congenic mice. 1 x 10^7 CD45.1$^+$ whole BM cells from WT mice were transplanted into non-irradiated 8-week-old CD45.2$^+$ control (*Ctrl*) or *Sel1l*^{Vav} KO mice. **d**, Percentage of donor derived (CD45.1$^+$) cells in the peripheral blood of non-irradiated Ctrl or *Sel1l*^{Vav} KO recipient mice at indicated time points. *n* = 5. **e**, Percentage of donor-derived (CD45.1$^+$) HSCs in the bone marrow of non-irradiated control or *Sel1l*^{Vav} KO recipient mice at 16 weeks after transplantation. *n* = 5. **f**, Experimental schematic of the transplantation of CD45.1$^+$ donor whole BM cells into lethally irradiated CD45.2$^+$ control (*Ctrl*) or *Sel1l*^{Vav} KO mice. Donor chimerism was analyzed 24 weeks after transplantation. **g**, Frequencies of donor derived WT HSCs are similar in the BM of irradiated *Ctrl* and *Sel1l*^{Vav} KO recipient mice. Frequencies (**left**) and numbers (**right**) of donor derived HSCs in the BM of recipient control (*Ctrl*) or *Sel1l*^{Vav} KO mice were analyzed by flow cytometry. *Ctrl*: *n* = 4; *Sel1l*^{Vav} KO: *n* = 5. *n* means independent mice. Two-sample Kolmogorov–Smirnov test (**b**), two-way ANOVA (**d**), or two-tailed Student's t-tests (**e**, **g**) was used to calculate all the *P* values. In **b**, **d**, and **e**, results are shown as mean ±
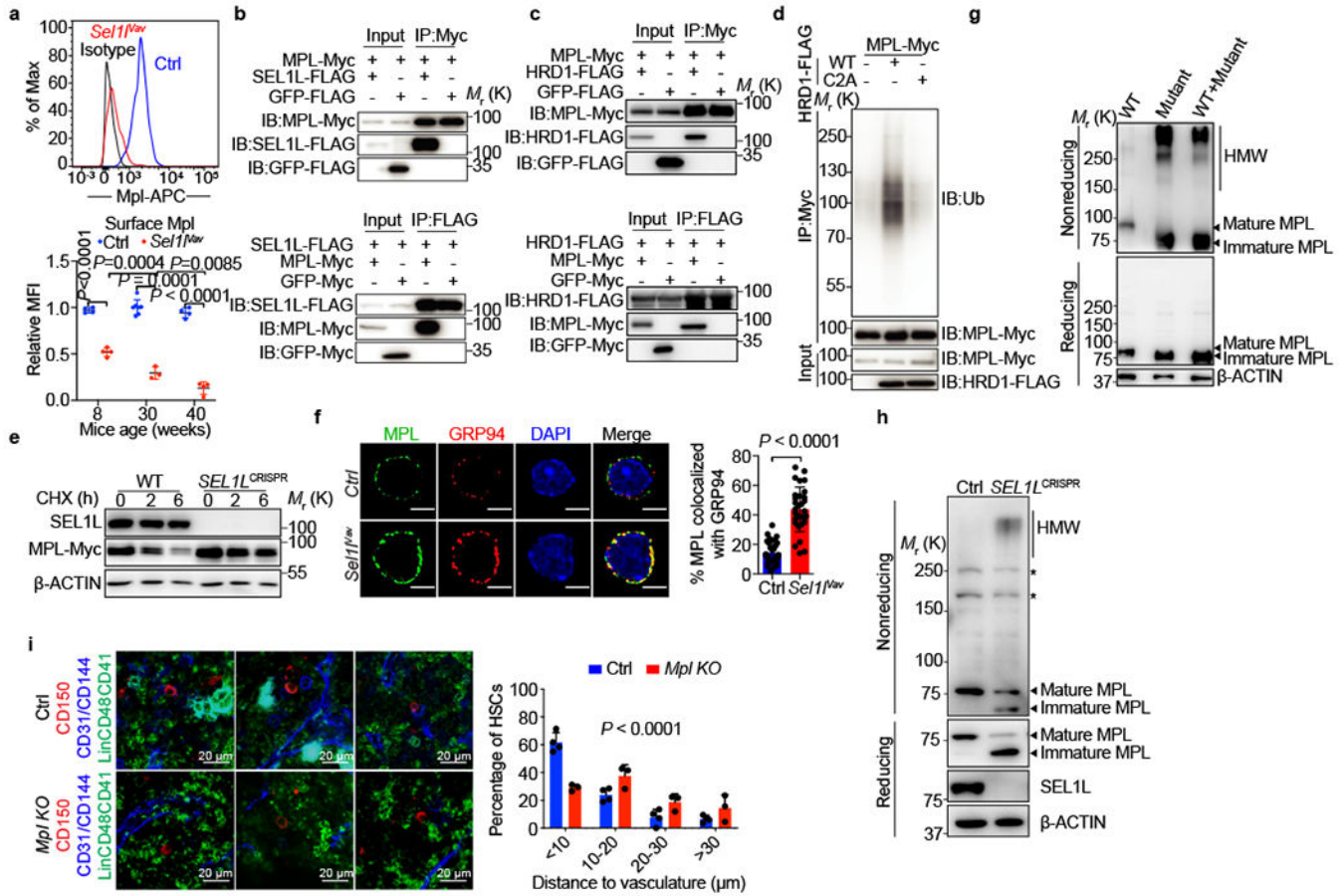
s.d. In **g**, results are shown as mean ± SEM. Statistical information is provided as source data.

Figure 4 |. SEL1L regulates MPL maturation.

a, Representative flow cytometry plots (**upper**) and quantification (**lower**) of surface MPL expression in *Ctrl* or S*el1l^Vav*-KO HSCs at indicated ages. MFI, mean fluorescence intensity. Week 8 and 40: $n = 4$; week 30, *Ctrl*: $n = 7$, S*el1l^Vav*-KO: $n = 7$. **b**, SEL1L interacts with MPL. Co-immunoprecipitation was performed with anti-Myc (**upper**) or anti-FLAG antibody (**lower**). IP: immunoprecipitation; IB: immunoblotting. **c**, HRD1 interacts with MPL. Co-immunoprecipitation was performed with anti-Myc (**upper**) or anti-FLAG antibody (**lower**). MG132 (10 μM) was added into culture medium 6 hours before harvest. **d**, MPL is ubiquitinated by HRD1. 293T cells were transfected with indicated plasmids were subjected to immunoprecipitation with anti-Myc antibody in denatured condition. The immunoblot was probed with anti-Ub antibody. **e**, Western blot analysis of MPL decay in cycloheximide (CHX)-treated WT or *SEL1L^CRISPR*-KO 293T cells at indicated time points. **f**, MPL protein is retained in the ER in the absence of SEL1L. Representative images (**left**) and quantification (**right**) of MPL that colocalized with exclusive ER-resident protein GRP94 in primary HSCs from 8-week-old *Ctrl* or *Sel1l^Vav*-KO mice. n=30 HSCs from Ctrl or *Sel1l^Vav*-KO mice were analyzed. Scale bar, 3 μm. **g**, Western blot analysis of Myc-tagged MPL in 293T cells transfected with Myc-tagged wildtype MPL (WT) or Myc-tagged mutant MPL (Mut) under reducing (with DTT) or non-reducing (without DTT) conditions. HMW, high molecular weight. **h**, WT MPL forms HMW aggregates in *SEL1L^CRISPR*-KO 293T cells. Western blot analysis of HA-tagged WT-MPL in WT or *SEL1L^CRISPR*-KO 293T cells

under reducing (with DTT) and non-reducing (without DTT) conditions. * indicates unspecific band. **i**, Representative 2D images (**left**) and quantification (**right**) of the distances between HSCs (CD150$^+$Lin$^-$CD48$^-$CD41$^-$, Red) and the closest vascular structure (CD31$^+$ and/or CD144$^+$, Blue). Ctrl: $n = 4$ independent experiments, *Mpl* KO: $n = 3$ independent experiments. In **a**, **f** and **i**, results are shown as mean ± s.d. Two-tailed Student's t-tests (**f**), two-way ANOVA (**a**) or two-sample Kolmogorov–Smirnov (**i**) test were used to assess the statistical significance. Statistical information and unprocessed blots are provided as source data.
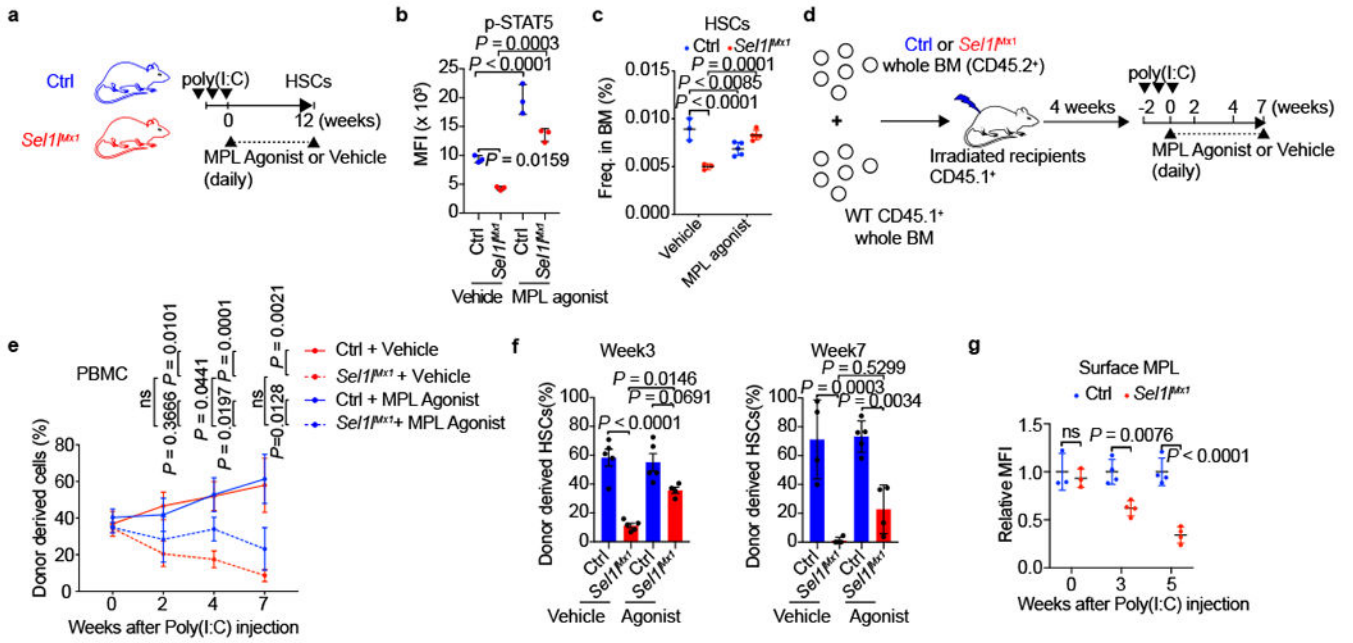
Figure 5 |. MPL agonist partially rescues the phenotypes of *Sel1l*-KO HSCs.

a, Schematic depiction of the rescue experiment with MPL agonist in *Ctrl* or *Sel1l*^Mx1^ mice. **b**, MPL agonist restores MPL downstream STAT5 phosphorylation in *Sel1l*^Mx1^ KO HSCs 12 weeks after poly(I:C) injection. $n = 3$. **c**, MPL agonist partially rescues steady-state HSCs in *Sel1l*^Mx1^ KO mice 12 weeks after poly(I:C) injection. Vehicle: $n = 3$; MPL agonist: $n = 5$. **d**, Schematic depiction of the competitive BMT rescue experiment with MPL agonist. **e**, MPL agonist partially rescues the reconstitution capacity of *Sel1l*^Mx1^ KO HSCs under BM transplantation condition. Frequency of donor derived PBMCs at indicated time points were analyzed by flow cytometry. $n = 4$ except for week 7. *Sel1l*^Mx1^+ Vehicle and *Sel1l*^Mx1^ + MPL agonist at week 7: $n = 3$. **f**, MPL agonist partially rescues the donor derived *Sel1l*^Mx1^ KO HSCs in the BM of irradiated recipient mice at indicated time points. Percentages of donor derived HSCs at week 3 and week 7 after poly(I:C) injection were analyzed by flow cytometry. Week 3: $n = 5$ except for *Sel1l*^Mx1^+ MPL agonist ($n = 4$); week 7: n = 4 except for *Ctrl* + MPL agonist ($n = 5$). **g**, Surface MPL expression in donor-derived *Ctrl* or *Sel1l*^Mx1^ KO HSCs in the recipient mice at indicated time points. Week 0: $n = 3$; Week 3/5: $n = 4$. In **b**, **c**, **f** and **g**, results are shown as mean ± s.d. In **e**, results are shown as mean ± s.e.m. One-way ANOVA (**e**) or two-way ANOVA (**b**, **c**, **f**, **g**) were used to assess statistical significance. ns, not significant. Statistical information is provided as source data.